

PULSAR KICKS AND SPIN TILTS IN THE CLOSE DOUBLE NEUTRON STARS PSR J0737-3039, PSR B1534+12 AND PSR B1913+16

B. WILLEMS, V. KALOGERA, AND M. HENNINGER

Northwestern University, Department of Physics and Astronomy, 2145 Sheridan Road, Evanston, IL 60208, USA

Draft version November 18, 2018

ABSTRACT

In view of the recent measurement of the scintillation velocity for PSR J0737-3039, we examine the complete set of constraints imposed on the pulsar B natal kicks (magnitude and orientation) and predict the most favorable pulsar kick velocity and spin tilt for both isotropic and polar kicks. Our analysis takes into account both currently unknown parameters: the orientation of the orbital plane on the sky (Ω) and the radial component of the systemic velocity (V_r). Assuming that the system's peculiar velocity is entirely due to the second supernova explosion, we find that the system may have crossed the Galactic plane multiple times since the birth of the second neutron star and that the post-supernova peculiar velocity could have been as high as $\simeq 1200 \text{ km s}^{-1}$. We also confirm the absolute lower and upper limits on the physical parameters derived in our earlier study. For specific combinations of the two unknown parameters Ω and V_r , however, we find much tighter constraints on the pre-supernova binary configuration and natal kicks imparted to pulsar B, as well as on the age of system. Once Ω is measured in the coming year, it will be straightforward to use the results presented here to further constrain the natal kicks and the spin-tilt predictions. We complete our comprehensive study and derive similar constraints and spin-tilt predictions for PSR B1534+12, where the only free parameter is V_r . Lastly, for PSR B1913+16, we update the progenitor and kick constraints using the measured pulsar spin tilt and allowing for Roche-lobe overflow from the progenitor of the pulsar companion.

Subject headings: Stars: Binaries: Close, Stars: Pulsars: General, Stars: Neutron, Stars: Pulsars: Individual: (PSR J0737-3039, PSR B1534+12, PSR B1913+16)

1. INTRODUCTION

The recent discovery of a unique, strongly relativistic binary pulsar (Burgay et al. 2003) that is also the first eclipsing, double pulsar system found in our Galaxy (Lyne et al. 2004) promises to provide us with more impressive tests of general relativity than ever before (Kramer 2004), to greatly improve our understanding of magnetospheric and pulsar emission physics (Lyutikov 2004; McLaughlin et al. 2004; Demorest et al. 2004; Granot & Mészáros 2004; Arons et al. 2004), and possibly indicates a realistic chance for the detection of gravitational waves from double-neutron-star (DNS) inspiral with the first-generation of ground-based interferometers (Kalogera et al. 2004; Kim et al. 2004).

Apart from the binary pulsar and eclipsing behavior, PSR 0737-3039 sets the current records for DNS properties: for example, it has the shortest spin and orbital period, smallest eccentricity, lowest magnetic field, and fastest apsidal motion. The measured current orbital parameters and masses along with an estimate of the system's age have allowed the careful account of its recent evolutionary history, since the time just before the supernova (SN) that formed pulsar B, the current companion to the millisecond pulsar A (Willems & Kalogera 2004; Dewi & van den Heuvel 2004). In Willems & Kalogera (2004) (hereafter Paper I), we found that the pre-SN binary¹ most likely consisted of the first-formed

NS and a Roche-lobe-filling helium star with mass between $2.1 M_\odot$ and $4.7 M_\odot$ (cf. Dewi & van den Heuvel 2004). The pre-SN orbital separation can be constrained between $1.36 R_\odot$ and $1.72 R_\odot$, and the magnitude of the kick velocity between 60 km s^{-1} and 1560 km s^{-1} .

Most recently, scintillation observations of pulsar A have allowed the measurement of the two systemic velocity components in the reference frame of the orbital plane projected on the sky (Ransom et al. 2004). This measurement gives us the first glimpse of the kinematic evolutionary history (in addition to that related to binary evolution). Therefore we extend the analysis presented in Paper I and take a comprehensive approach to constraining the formation of PSR J0737-3039. The concept is similar to that adopted by Wex, Kalogera, & Kramer (2000) with two main differences: (i) at present there is no constraint on pulsar A's spin tilt from timing or polarization observations; (ii) the current kinematic measurements involve two free parameters, the orientation of the orbital plane on the sky (Ω) and the radial component of the systemic velocity (V_r).

In this paper, we account for the complete set of equations describing the formation of PSR J0737-3039 and derive constraints on the progenitor of pulsar B and on the kicks (both isotropic and polar) imparted to it at birth. We also derive predictions for the possible orientation of pulsar A's spin axis with respect to the current orbital angular momentum axis. We carefully analyze and present the dependence of these results on Ω and V_r and on the system's age. The measurement of Ω along with proper motion components is anticipated in the coming year. We show that such measurements can be used with

Electronic address: b-willems, vicky@northwestern.edu, m-henninger@alumni.northwestern.edu

¹ Throughout the paper, we use the terms pre- and post-SN to refer to the instants just before and right after the SN explosion forming the second NS.

TABLE 1
PARAMETERS OF PSR J0737-3039, PSR B1534+12, AND PSR B1913+16.

Parameter	Notation	PSR J0737-3039 ^a	PSR B1534+12 ^b	PSR B1913+16 ^c
Right Ascension (J2000)	α	07 ^h 37 ^m 51.25 ^s	15 ^h 37 ^m 09.96 ^s	19 ^h 15 ^m 28.00 ^s
Declination (J2000)	δ	-30°39'40.74''	11°55'55.55''	16°06'27.40''
Proper motion in R.A.	μ_α (mas yr ⁻¹)	-	1.34 ± 0.01	-3.27 ± 0.35
Proper motion in Decl.	μ_δ (mas yr ⁻¹)	-	-25.05 ± 0.02	-1.04 ± 0.42
Galactic longitude (J2000)	l	245°2	19°8	50°0
Galactic latitude (J2000)	b	-4°5	48°3	2°1
Proper motion in Gal. long.	μ_l (mas yr ⁻¹)	-	-21.57 ^d	-0.60
Proper motion in Gal. lat.	μ_b (mas yr ⁻¹)	-	-12.80 ^d	-3.38
Distance	d (kpc)	~ 0.6	1.02 ± 0.05	8.3 ± 1.4
Characteristic age of the ms pulsar	τ_c (Myr)	210	250	110
Spin-down age of the ms pulsar	τ_b (Myr)	100	210	80
Mass of the ms pulsar	M_A (M_\odot)	1.34	1.33	1.44
Mass of the companion	M_B (M_\odot)	1.25	1.35	1.39
Current semi-major axis	A_{cur} (R_\odot)	1.26	3.28	2.80
Current orbital eccentricity	e_{cur}	0.0878	0.274	0.617

^aBurgay et al. 2003; Lyne et al. 2004.

^bWolszczan 1991; Stairs et al. 2002; Konacki, Wolszczan, & Stairs 2003; Arzoumanian, Cordes, & Wasserman 1999.

^cHulse & Taylor 1975; Taylor et al. 1976; Taylor, Fowler, & McCulloch 1979; Taylor & Weisberg 1982, 1989; Damour & Taylor 1991; Arzoumanian et al. 1999, Wex et al. 2000.

^dDerived quantities.

the results presented here to derive tighter constraints. We also compare our predicted spin tilts with those derived based on the geometric model of Jenet & Ransom (2004) for pulsar B's eclipses and find excellent agreement. We note that our predicted spin tilts can also be used along with polarization observations to anticipate the most likely timing of pulsar A's disappearance due to geodetic precession as a function of the radial velocity (which in the long term will be the only remaining unknown property) of the system.

In addition to PSR J0737-3039 (Section 2), we analyze our current understanding of the evolutionary history of the other two close currently known DNS systems in the Galaxy. For PSR B1534+12, we use the masses, orbital characteristics, and measured proper motion to derive progenitor and kick constraints, as well as spin tilt predictions (Section 3). For PSR B1913+16, we extend the analysis of Wex et al. (2000) to take into account the possibility that the helium star progenitor of the pulsar companion could have been filling its Roche lobe. We also derive the probability distributions of the kick magnitude imparted to the last-born NS (Section 4). We end with a summary of our main conclusions, a discussion of the implications of our analysis for the relation of kicks to spin orientations, and a comparison of our results with other recent studies.

2. THE RECENT EVOLUTIONARY HISTORY OF PSR J0737-3039

In this Section, we use the scintillation velocities measured by Ransom et al. (2004) to first determine the spatial velocity of PSR J0737-3039 with respect to a frame of reference locked to the Galaxy and next follow the motion of the system in the Galaxy backwards in time until the time of its formation. We identify crossings of the Galactic plane as possible birth sites and, by subtracting the local Galactic rotational velocity from the total systemic velocity at birth, determine the system's post-SN peculiar velocity. This velocity is subsequently used to tighten the progenitor constraints derived in Paper I.

The physical parameters of PSR J0737-3039 relevant to this investigation are summarized in Table 1. We particularly note that we use the estimate $\tau_b = 100$ Myr of the time since pulsar A left the maximum spin-up line as an *upper limit* for the age of the system (for details, see Paper I).

2.1. Present Systemic Velocity

The interstellar scintillation measurements carried out by Ransom et al. (2004) yield two of the three systemic velocity components required to describe the space motion of PSR J0737-3039. Both components are measured in the plane perpendicular to the line-of-sight and with respect to the Earth. The first one has a magnitude of $\simeq 96.6 \pm 3.7$ km s⁻¹ and is directed along the line connecting the ascending and descending node of the pulsar's orbit, while the second one has a magnitude of $\simeq 103.1 \pm 7.7$ km s⁻¹ and is directed perpendicular to the nodal line. In what follows, we will refer to these two components as V^\parallel and V^\perp , respectively. Since the statistical errors of 3.7 km s⁻¹ and 7.7 km s⁻¹ do not account for unknown systematic errors, we here adopt the values $V^\parallel = 100$ km s⁻¹ and $V^\perp = 110$ km s⁻¹, and assume an uncertainty on both components of ± 20 km s⁻¹ (Ransom 2004, private communication).

Before we pass on from the scintillation velocity components to velocity components with respect to a frame of reference locked to the Galaxy, it is interesting to examine the velocity components V_α and V_δ , and the corresponding proper motion components μ_α and μ_δ , in right ascension (α) and declination (δ). The velocity components V_α and V_δ are obtained from V^\parallel and V^\perp by means of the transformation formulae

$$\left. \begin{aligned} V_\alpha &= V^\parallel \cos \Omega - V^\perp \sin \Omega, \\ V_\delta &= V^\parallel \sin \Omega + V^\perp \cos \Omega, \end{aligned} \right\} \quad (1)$$

where Ω is the *unknown* longitude of the ascending node measured right-handed around the line-of-sight, from the

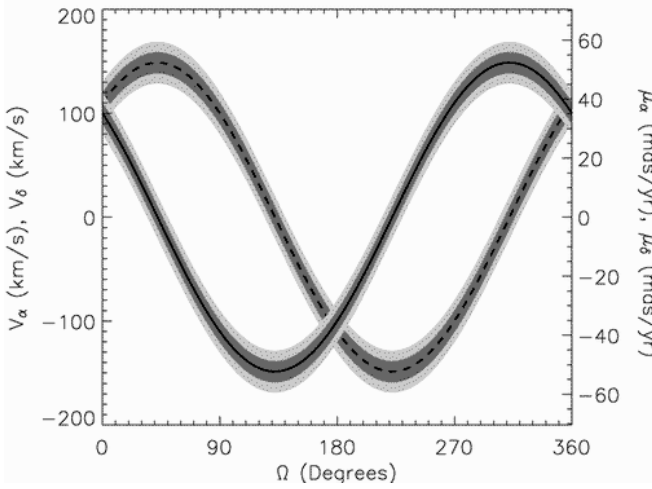


FIG. 1.— Variation of the velocity components of PSR J0737-3039 in right ascension α (solid lines) and declination δ (dashed lines) as a function of the unknown longitude of the ascending node Ω . The dark and light gray bands indicate the errors in V_α and V_δ corresponding to errors of 10 and 20 km s⁻¹ in the scintillation velocity components V^\parallel and V^\perp . The right-hand axis shows the magnitude of the proper motion components μ_α and μ_δ , for a distance of 0.6 kpc.

East through the North. The proper motion components $\mu_\alpha = \cos \delta d\alpha/dt$ and $\mu_\delta = d\delta/dt$ are then given by the relations

$$\left. \begin{aligned} \frac{V_\alpha}{\text{km s}^{-1}} &= 4.74 \left(\frac{d}{\text{kpc}} \right) \left(\frac{\mu_\alpha}{\text{mas yr}^{-1}} \right), \\ \frac{V_\delta}{\text{km s}^{-1}} &= 4.74 \left(\frac{d}{\text{kpc}} \right) \left(\frac{\mu_\delta}{\text{mas yr}^{-1}} \right), \end{aligned} \right\} \quad (2)$$

where d is the distance of the binary from the Sun.

The variations of V_α (or μ_α) and V_δ (or μ_δ) are shown in Fig. 1 as a function of the unknown Ω . The dark and light gray bands indicate the errors in V_α (or μ_α) and V_δ (or μ_δ) corresponding to errors of 10 and 20 km s⁻¹ in V^\parallel and V^\perp . The magnitude of V_α and V_δ ranges from approximately -175 km s⁻¹ to 175 km s⁻¹, while, for a distance of 0.6 kpc, the magnitude of μ_α and μ_δ can be anywhere between -60 mas yr⁻¹ and 60 mas yr⁻¹ (see also Ransom et al. 2004). A 100 mas proper motion should then be detectable in less than 2 years time. It is furthermore clear that, even with the extended error bars of ± 20 km s⁻¹, future measurements of the proper motion will considerably constrain the possible values of the longitude of the ascending node Ω .

Since the scintillation velocity measurements only give the magnitude of V^\parallel and V^\perp , the motion of the binary projected on the plane perpendicular to the line-of-sight should, in principal, be considered in four different directions corresponding to four different combinations of $V^\parallel = \pm 100$ km s⁻¹ and $V^\perp = \pm 110$ km s⁻¹. This additional degree of freedom may however be incorporated in the unknown longitude of the ascending node. To illustrate this, we consider two sets of scintillation velocity components $(V_1^\parallel, V_1^\perp)$ and $(V_2^\parallel, V_2^\perp)$ whose orientations in the plane perpendicular to the line-of-sight are determined by the angles Ω_1 and Ω_2 . From Eqs. (1), it then follows that the two sets of scintillation velocity components give rise to equal velocity components in right

ascension and declination when $\Omega_2 = \Omega_1 + \Delta\Omega$, where $\Delta\Omega$ is determined by

$$\left. \begin{aligned} \cos(\Delta\Omega) &= \frac{V_1^\parallel}{V_2^\parallel} + \frac{V_2^\perp}{V_2^\parallel} \frac{V_1^\perp V_2^\parallel - V_1^\parallel V_2^\perp}{(V_2^\parallel)^2 + (V_2^\perp)^2}, \\ \sin(\Delta\Omega) &= \frac{V_1^\perp V_2^\parallel - V_1^\parallel V_2^\perp}{(V_2^\parallel)^2 + (V_2^\perp)^2}. \end{aligned} \right\} \quad (3)$$

Hence, the cases $(V^\parallel, V^\perp) = (-100 \text{ km s}^{-1}, 110 \text{ km s}^{-1})$, $(V^\parallel, V^\perp) = (100 \text{ km s}^{-1}, -110 \text{ km s}^{-1})$, and $(V^\parallel, V^\perp) = (-100 \text{ km s}^{-1}, -110 \text{ km s}^{-1})$, can be obtained from the case $(V^\parallel, V^\perp) = (100 \text{ km s}^{-1}, 110 \text{ km s}^{-1})$ by translating Ω over angles of 275.5°, 95.5°, and 180°, respectively. For the remainder of the paper, we therefore restrict ourselves to presenting the results associated with the velocity components $V^\parallel = 100 \text{ km s}^{-1}$ and $V^\perp = 110 \text{ km s}^{-1}$.

2.2. Kinematic History and Age

In order to trace the Galactic motion of PSR J0737-3039 back in time until the time of its formation, we first need to determine the three velocity components of the current systemic velocity in a reference frame locked to the Galaxy. For this purpose, we choose a right-handed frame $OXYZ$ with the origin at the Galactic center and with the XY -plane coinciding with the Galactic plane. We adopt the direction from the Sun to the Galactic center as the positive direction of the X -axis and the direction of the Sun's motion due to the Galactic rotation as the positive direction of the Y -axis.

The components (V_X, V_Y, V_Z) of the current systemic velocity with respect to $OXYZ$ are obtained by the vector transformation

$$\begin{pmatrix} V_X \\ V_Y \\ V_Z \end{pmatrix} = \vec{V}_\odot + J \cdot \begin{pmatrix} V_r \\ V_\alpha \\ V_\delta \end{pmatrix}, \quad (4)$$

where \vec{V}_\odot is the Galactic velocity of the Sun, $J = \partial(X, Y, Z)/\partial(d, \alpha, \delta)$ is the Jacobian of the coordinate transformation linking (X, Y, Z) to (d, α, δ) , and V_r is the *unknown* radial velocity. The Galactic velocity of the Sun in turn is the vector sum of the Sun's circular velocity around the Galactic center and the Sun's peculiar velocity with respect to the local standard of rest:

$$\vec{V}_\odot = \begin{pmatrix} 0 \text{ km s}^{-1} \\ 221 \text{ km s}^{-1} \\ 0 \text{ km s}^{-1} \end{pmatrix} + \begin{pmatrix} 10 \text{ km s}^{-1} \\ 5 \text{ km s}^{-1} \\ 7 \text{ km s}^{-1} \end{pmatrix}, \quad (5)$$

(Binney & Dehnen 1997, Bienaymé 1999). It is evident from Eqs. (1) and (4) that the kinematic evolution of PSR J0737-3039 depends on two unknown parameters: Ω and V_r .

The variations of V_X and V_Z as functions of Ω are displayed in Fig. 2, for $V_r = -1500, -1250, -1000, \dots, 1500 \text{ km s}^{-1}$. It is interesting to note that for $V_r \lesssim -250 \text{ km s}^{-1}$, V_X is always positive so that the motion of the system backwards in time is away from the Galactic center. In addition, for $\Omega \lesssim 25^\circ$ and $\Omega \gtrsim 300^\circ$, V_Z is positive for all considered values of V_r so that the motion of the system backwards in time is also away from the Galactic plane. As we will see below, this behaviour together with the current position of the system below the

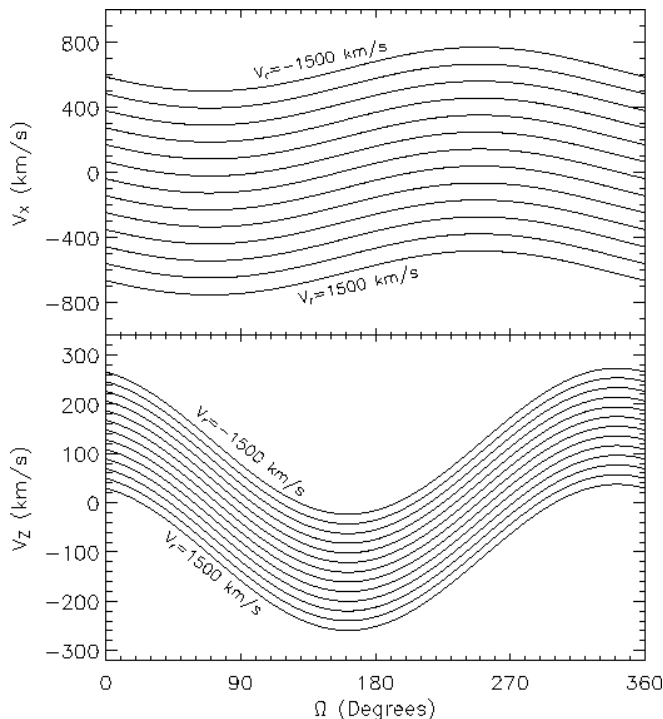


FIG. 2.— Variation of the velocity components V_X and V_Z of PSR J0737-3039 as a function of the unknown longitude of the ascending node Ω , for V_r -values ranging from -1500 to 1500 km s^{-1} in increments of 250 km s^{-1} .

Galactic plane has important consequences for the past motion of PSR J0737-3039 in the Galactic potential and the identification of possible birth places.

Given the present position and velocity components of PSR J0737-3039 in the adopted reference frame, we integrate the equations governing the system's motion in the Galaxy backwards in time and look for possible birth sites as a function of Ω and V_r . Since DNS systems are thought to form from primordial binaries with initially two massive component stars, which are known to have a very small vertical scale height of $50\text{--}70 \text{ pc}$, we assume the primordial binary to be born in the Galactic disk. Wex et al. (2000) furthermore noted that both the orbital velocity before the birth of the first NS and the center-of-mass velocity imparted to the system due to the first SN explosion are typically of the order of only a few 10 km s^{-1} (see also Brandt & Podsiadlowski 1995; Pfahl et al. 2002). However, Pfahl et al. (2002) used a population synthesis technique to construct a probability distribution of post-SN peculiar velocities of high-mass X-ray binaries and found a low-probability tail extending all the way up to $\simeq 200 \text{ km s}^{-1}$. The possibility that the first SN explosion in PSR J0737-3039 produced a kick of a few 100 km s^{-1} to the binary's center-of-mass can therefore not be entirely ruled out. In order to properly treat these cases, the effect of both the first and second SN explosion on the space motion of the binary must be taken into account, which requires the introduction of three additional free parameters (magnitude of the first SN kick, direction of the first SN kick relative to that of the second kick, and time expired between the two kicks). In view of this added complexity and the low probability of the high systemic velocities after the first SN explo-

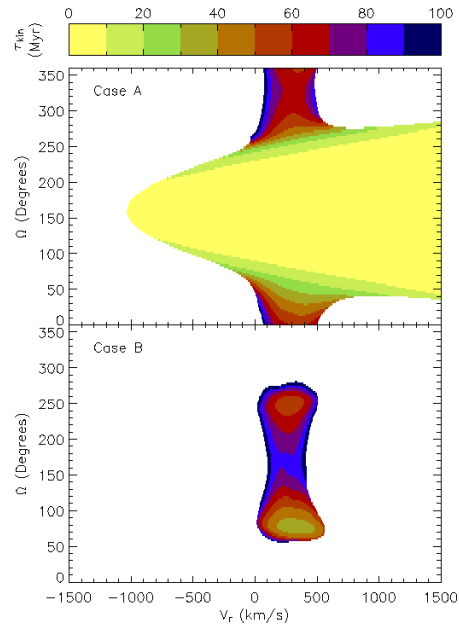


FIG. 3.— Kinematic age of PSR J0737-3039 as a function of the unknown radial velocity V_r and the unknown longitude of the ascending node Ω , for both case A (top panel) and B (bottom panel).

sion, we here leave aside these more complicated and rarer cases and assume the present kinematic properties of PSR J0737-3039 to be entirely due to the second SN explosion. In particular, we assume that the system was still close to the Galactic plane at the time of the second SN explosion and that its pre-SN *peculiar* velocity was small in comparison to the Galactic rotational velocity at the formation site. The post-SN systemic velocity of the binary is then given by the sum of the local Galactic rotational velocity and the peculiar velocity due to the second SN explosion.

Following Wex et al. (2000), we use the Galactic potential of Kuijken & Gilmore (1989) to calculate the motion of PSR J0737-3039 in the Galaxy backwards in time for all possible Ω -values between 0° and 360° , and V_r -values between -1500 and 1500 km s^{-1} . Each time the binary crosses the Galactic plane ($Z=0$), we check whether the crossing occurred less than 100 Myr in the past and whether the crossing point is within 15 kpc from the Galactic center. If so, the crossing is considered as a possible birth site and the post-SN peculiar velocity V_{pec} is determined by subtracting the local Galactic rotational velocity from the system's total systemic velocity².

In cases where the binary crosses the Galactic plane within 1 kpc from the Galactic center, we assume that the pre-SN binary belonged to the disk-like component of the Galactic bulge (see, e.g., Kuijken & Rich 2002). Since the time required by a massive binary to evolve into a DNS is at most of the order of $\sim 20 \text{ Myr}$, much smaller than the typical age of 'pure' Galactic bulge stars, we exclude

² Note that Table 3 in Wex et al. (2000) contained an error in the coefficients β_1 for $A = 2, 3$; where the correct values are $\beta_1 = 0$ for both $A = 2$ and 3 . We corrected this error and confirmed that it does not quantitatively affect the results presented by Wex et al. (2000) for PSR B1913+16 (see also Section 4). In particular, the resulting relative errors on the times of the Galactic plane crossings and the associated peculiar velocities are less than $\sim 6\%$.

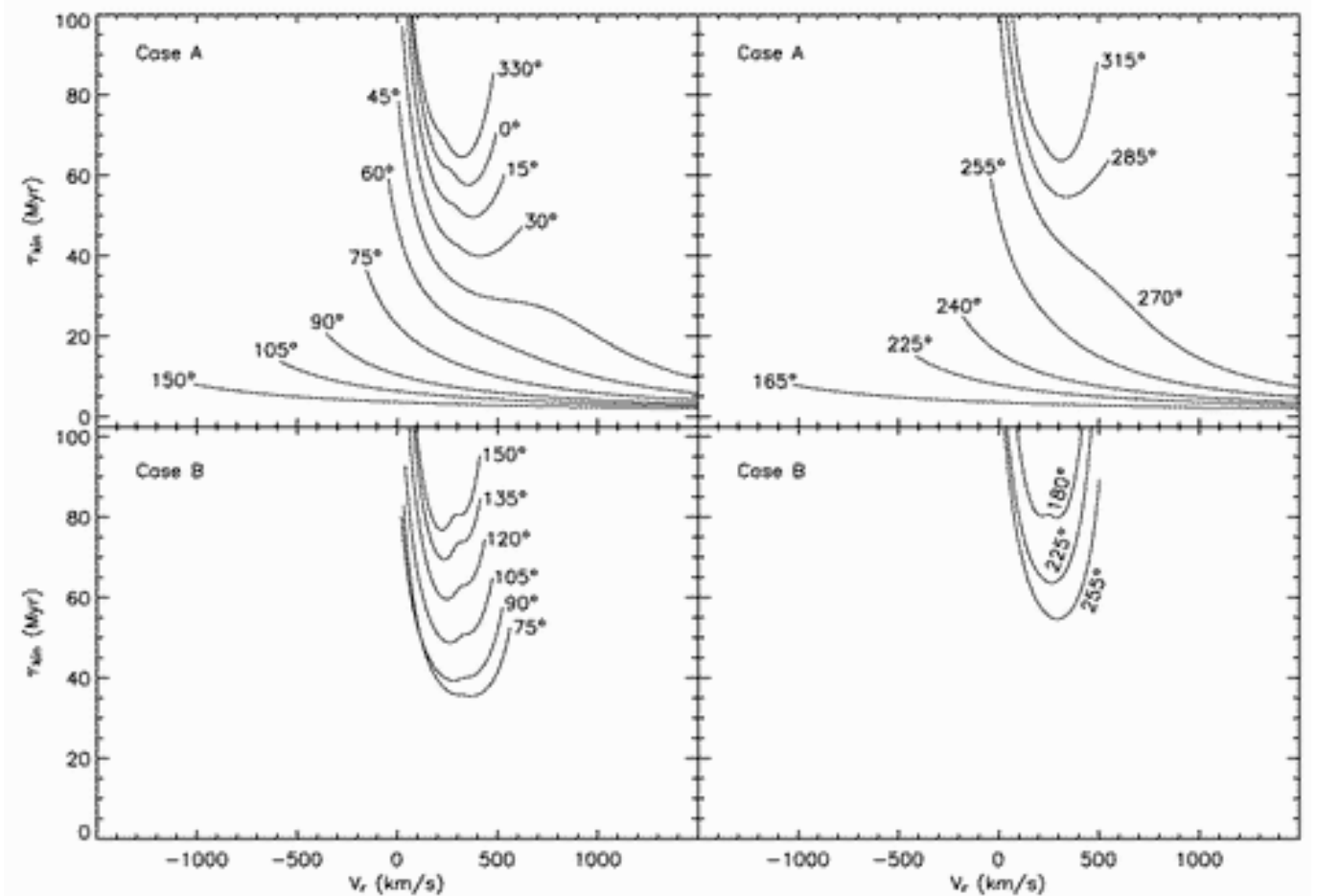


FIG. 4.— Cross sections of Fig. 3 showing the variation of the kinematic age τ_{kin} of PSR J0737-3039 as a function of V_r , for different values of Ω . The top and bottom panels correspond to case A and B, respectively.

birth sites in the bulge at $Z \neq 0$. Hence, all disk crossings within 100 Myr in the past and within 15 kpc from the Galactic center are considered as possible birth sites and are assumed to follow the disk-like rotation curve determined by the adopted Galactic potential.

The time in the past at which the system crosses the Galactic disk provides an estimate for the time since the formation of the DNS. Since some of the Galactic trajectories cross the Galactic plane more than once, these kinematic ages are not uniquely determined by Ω and V_r . In particular, for $0 \text{ km s}^{-1} \lesssim V_r \lesssim 550 \text{ km s}^{-1}$ and $60^\circ \lesssim \Omega \lesssim 280^\circ$, we find that the system may have crossed the Galactic plane twice within the last 100 Myr; while for $50 \text{ km s}^{-1} \lesssim V_r \lesssim 400 \text{ km s}^{-1}$ and $240^\circ \lesssim \Omega \lesssim 265^\circ$ it may have even crossed the Galactic plane as much as three times. Since the latter situation only occurs for just a few, greatly fine-tuned trajectories at ages very close to the adopted upper limit of 100 Myr, we leave aside these rather rare cases and focus on the first and second Galactic plane crossings. We will refer to these crossings as case A and case B, respectively.

The dependence of the kinematic age τ_{kin} on both Ω and V_r is displayed in Figs. 3 and 4: Fig. 3 shows the kinematic ages for all considered Ω - and V_r -values using a linear gray scale (color in the electronic edition), while Fig. 4 gives a more detailed view of the dependence of

τ_{kin} on V_r for some specific values of Ω .

For case A, the majority of the Galactic disk crossings occur less than 20 Myr in the past. These young ages are associated with longitudes of the ascending node between $\simeq 30^\circ$ and $\simeq 260^\circ$, and radial velocities larger than approximately -1000 km s^{-1} . Galactic disk crossings occurring more than 20 Myr in the past are typically associated with Ω -values smaller than $\simeq 70^\circ$ or larger than $\simeq 230^\circ$, and with V_r -values between -200 km s^{-1} and 700 km s^{-1} . The range of possible V_r -values becomes narrower with increasing kinematic ages and is most restricted when the age of the system is close to the adopted upper limit of 100 Myr. There are furthermore almost no disk crossings associated with negative V_r -values when $\tau_{kin} \gtrsim 20 \text{ Myr}$. The origin of this systematic behavior is related to the dependence of the X - and Z -components of the current peculiar velocity on V_r and Ω (see Fig. 2): the Galactic position of the system is such that negative V_r -values correspond to orbits where the first disk crossing occurs either too far in the past (in excess of even the characteristic age of 210 Myr) or too far away from the Galactic center (at radii in excess of 15 kpc). The disk crossings associated with negative V_r -values and $\tau_{kin} \lesssim 20 \text{ Myr}$ occur due to the suitable orientation of the orbit in space: the Ω -values ($60^\circ \lesssim \Omega \lesssim 230^\circ$) are such that the Z -component of the current peculiar velocity is negative,

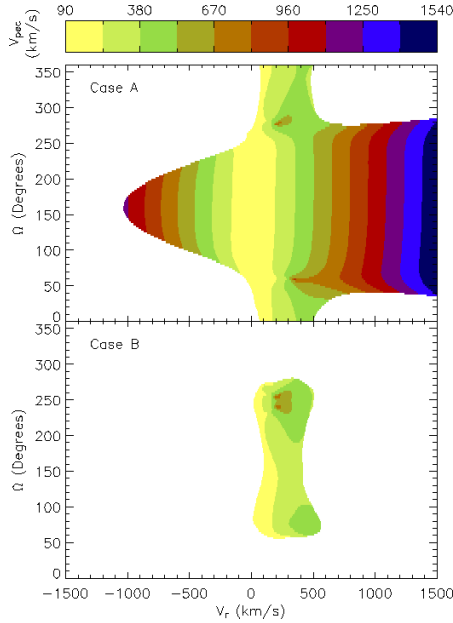


FIG. 5.— Peculiar velocity of PSR J0737-3039 as a function of the unknown radial velocity V_r and the unknown longitude of the ascending node Ω . The top and bottom panels correspond to case A and B, respectively.

so that motion backwards in time is towards the Galactic plane. In addition, Lorimer et al. (2004) recently estimated the age of the system to be most likely between 30 Myr and 70 Myr. If the age is indeed so constrained, the range of possible Ω -values would be limited to $\Omega \lesssim 80^\circ$ and $\Omega \gtrsim 240^\circ$, and the range of possible V_r -values to $-200 \text{ km s}^{-1} \lesssim V_r \lesssim 800 \text{ km s}^{-1}$. In view of the current uncertainties we will perform our analysis for the upper limit of 100 Myr, but the above age constraints may be kept in mind.

Case B disk crossings, on the other hand, only occur for V_r -values between 0 km s^{-1} and 550 km s^{-1} , and Ω -values between 60° and 280° . The associated kinematic ages are always longer than 20 Myr, so that constraining the age to 30–70 Myr does not impose severe additional limits on the ranges of Ω - and V_r -values.

In Fig. 5, we show the peculiar velocities V_{pec} associated with the Galactic plane crossings at ages shown in Fig. 3. The peculiar velocities range from 90 km s^{-1} to 1550 km s^{-1} and from 120 km s^{-1} to 800 km s^{-1} , for case A and B, respectively. However, when $\tau_{\text{kin}} \gtrsim 40 \text{ Myr}$, the post-SN peculiar velocities associated with case A are also confined to a smaller interval between 90 km s^{-1} and 800 km s^{-1} . In addition, for a given value of Ω , the peculiar velocity V_{pec} generally increases with increasing absolute values of V_r . In Section 2.3, we will use the post-SN peculiar velocities to further constraint the properties of the pre-SN progenitor of PSR J0737-3039 derived in Paper I.

We conclude this section by noting that, if PSR J0737-3039 is indeed born in the Galactic disk, Figs. 3 and 5 show that the future determination of Ω may yield important constraints on its age and post-SN orbital velocity, even without knowing the system's present radial velocity.

2.3. Progenitor Constraints

In this Section, we extend the analysis presented in Paper I by adding the kinematic history of PSR J0737-3039 to the constraints resulting from the orbital dynamics of asymmetric, instantaneous SN explosions. The two main differences with paper I are that (i) the problem is now expressed as a function of the two unknown parameters Ω and V_r , and (ii) the spin-down age $\tau_b = 100 \text{ Myr}$ is now used as an upper limit for the age instead of as an actual age estimate. The first difference implies that the constraints will also become functions of Ω and V_r , while the second difference affects the amount of orbital evolution that may have taken place since the birth of the system.

As in Paper I, we assume that the post-SN orbit evolved solely under the influence of gravitational radiation and determine the semi-major axis A and orbital eccentricity e right after the second SN explosion by numerically integrating the orbital evolution equations derived by Junker & Schäfer (1992) backwards in time. For each combination of Ω and V_r , the integration is terminated at the kinematic age τ_{kin} corresponding to a case A or case B Galactic disk crossing. The resulting post-SN orbital separations and orbital eccentricities range from $A = 1.26 R_\odot$ and $e = 0.088$ ($\tau_{\text{kin}} = 0 \text{ Myr}$) to $A = 1.54 R_\odot$ and $e = 0.12$ ($\tau_{\text{kin}} = 100 \text{ Myr}$).

Under the assumption that the pre-SN binary orbit is circular (see Paper I), the pre- and post-SN binary parameters are related by the conservation laws of orbital energy and orbital angular momentum. The relations take the form

$$V_k^2 + V_0^2 + 2 V_k V_0 \cos \theta = G (M_A + M_B) \left(\frac{2}{A_0} - \frac{1}{A} \right), \quad (6)$$

$$A_0^2 [V_k^2 \sin^2 \theta \cos^2 \phi + (V_k \cos \theta + V_0)^2] = G (M_A + M_B) A (1 - e^2) \quad (7)$$

(e.g., Hills 1983; Kalogera 1996), where G denotes the gravitational constant, A_0 the pre-SN orbital separation, M_0 and $V_0 = [G (M_A + M_0) / A_0]^{1/2}$ the helium star's mass and pre-SN orbital velocity, and V_k the magnitude of the kick velocity imparted to pulsar B at birth. The angles θ and ϕ describe the direction of the kick velocity imparted to pulsar B: θ is the polar angle between \vec{V}_k and \vec{V}_0 , while ϕ is the corresponding azimuthal angle measured in the plane perpendicular to \vec{V}_0 so that $\phi = \pi/2$ coincides with the direction from pulsar A to pulsar B. For a given kick-velocity magnitude and a given set of pre- and post-SN binary parameters, the polar angle $\theta \in [0, \pi]$ is uniquely determined by Eq. (6). The azimuthal angle $\phi \in [0, 2\pi]$, on the other hand, is only determined through the square of its cosine so that, for a given kick-velocity magnitude, four solutions to Eqs. (6) and (7) exist for each set of pre- and post-SN binary parameters.

A necessary set of conditions for the existence of solutions of Eqs. (6) and (7) is that $0 \leq \sin^2 \theta \leq 1$ and $0 \leq \cos^2 \phi \leq 1$. Together with the requirements that the binary must remain bound after the SN explosion, that the post-SN orbit must pass through the position of both

stars at the time of the SN explosion, and that the SN kick must reproduce the post-SN orbital parameters A and e , these conditions impose strong constraints on the possible pre-SN values of A_0 and M_0 as well as on the magnitude of the kick velocity V_k that have already been described in detail in Paper I (see also Fryer & Kalogera 1997; Kalogera & Lorimer 2000). In addition to these constraints, the kick velocity and the pre- and post-SN binary parameters must now also be compatible with the post-SN peculiar velocity derived by following the motion of the system in the Galaxy backwards in time. From Eqs. (3) and (34) in Kalogera (1996), it follows that the post-SN peculiar velocity is related to the kick velocity and to the pre- and post-SN binary parameters as

$$V_{\text{pec}}^2 = \frac{M_B M_0}{(M_A + M_0)(M_A + M_B)} \left[\frac{G(M_0 - M_B)M_A}{M_0 A} + \frac{G(M_0 - M_B)(M_0 - 2M_B)M_A}{M_0 M_B A_0} + V_k^2 \right]. \quad (8)$$

We require the peculiar velocity obtained from this equation to be within the error bars of the peculiar velocity obtained by following the motion of the system backwards in time. In order to estimate the error bars on the latter, we neglect the contributions resulting from uncertainties in the adopted Galactic potential and assume them to be entirely due to the errors in the scintillation velocity measurements ($\pm 20 \text{ km s}^{-1}$).

In Figs. 6–8, we show the ranges of M_0 , A_0 , and V_k values satisfying *all* the imposed constraints as functions of the unknown radial velocity V_r , for case A and case B, and for different specific values of the longitude of the ascending node Ω . The parameter space for case A disk crossings is displayed in the upper 9 panels of the figures, whereas the parameter space for case B disk crossings is displayed in the lower 6 panels. The gray scale (color in the electronic edition) indicates the kinematic ages associated with different combinations of Ω and V_r (cf. Fig. 3).

For each value of Ω , there is a finite range of V_r -values leading to physically acceptable solutions for the pre-SN progenitor of PSR J0737-3039. For case A disk crossings, the range is widest for $\Omega \simeq 160^\circ$, where $-1000 \text{ km s}^{-1} \lesssim V_r \lesssim 1100 \text{ km s}^{-1}$. The actual range of V_r -values leading to physically acceptable solutions is therefore somewhat smaller than the range considered for the Galactic motion calculations presented in Section 2.2. For case B disk crossings, the V_r -range is widest when $\Omega \simeq 80^\circ$ or $\Omega \simeq 260^\circ$, where $0 \text{ km s}^{-1} \lesssim V_r \lesssim 550 \text{ km s}^{-1}$. Hence, for case B, the physical constraints on the progenitor of PSR J0737-3039 do not put any further constraints on the radial velocity besides those already found from the system's kinematic history (see Fig. 3).

In Paper I, the mass of pulsar B's helium star progenitor was constrained to be between $2.1 M_\odot$ and $4.7 M_\odot$. These limits correspond to the lowest mass for which a helium star is expected to form a NS and to the highest mass for which mass transfer from pulsar B's helium-star progenitor to pulsar A is expected to be dynamically stable. Despite the dependence of the analysis presented here on the two unknown parameters Ω and V_r , the range of possible M_0 -values is much more tightly constrained than in Paper I for many combinations of Ω and V_r . This particularly applies to (Ω, V_r) pairs for which the kine-

matic age is close to the age of 100 Myr adopted there (see, e.g., the case A solutions associated with $\Omega = 0^\circ$ and $80 \text{ Myr} \leq \tau_{\text{kin}} \leq 100 \text{ Myr}$ in Fig. 6). The range of available helium star masses M_0 furthermore tends to be most constrained for small values of the radial velocity.

For a given post-SN orbital separation A and eccentricity e , the possible values of the pre-SN orbital separation A_0 range from $A(1 - e)$ to $A(1 + e)$ (Flannery & van den Heuvel 1975). In Paper I, we used the values of A and e obtained by integrating the equations governing the orbital evolution due to gravitational radiation backwards in time up to an age of 100 Myr to constrain A_0 to be between $1.36 R_\odot$ and $1.72 R_\odot$. These small pre-SN orbital separations imply that the helium star progenitor of pulsar B is very likely overflowing its Roche lobe (see also Dewi & van den Heuvel 2004). Here we take into account that the age of PSR J0737-3039 may be shorter than 100 Myr. Consequently, the lower limit on A_0 may actually be even smaller than $1.36 R_\odot$ since less orbital evolution may have taken place. An absolute lower limit on A_0 is given by $A_{\text{cur}}(1 - e_{\text{cur}}) = 1.15 R_\odot$, corresponding to the lower limit associated with the post-SN orbital parameters for the minimum age $\tau_{\text{kin}} = 0 \text{ Myr}$. Since the increase in A and e due to the orbital evolution backwards in time is largest when $\tau_{\text{kin}} = \tau_b = 100 \text{ Myr}$, the value of $1.72 R_\odot$ provides an absolute upper limit on A_0 . Hence, for the pre-SN helium star mass range quoted above, the conclusion reached in Paper I that the immediate progenitor of pulsar B is most likely overflowing its Roche lobe remains valid. The range of possible pre-SN orbital separations associated with given values of Ω and V_r is furthermore *most restricted for the youngest kinematic ages* found: the width of the allowed interval is approximately $0.25 R_\odot$ when $\tau_{\text{kin}} \lesssim 20 \text{ Myr}$ and $0.36 R_\odot$ when $\tau_{\text{kin}} \simeq 100 \text{ Myr}$.

In Paper I we derived a constrained range for the kick-velocity magnitude between 60 km s^{-1} and 1560 km s^{-1} . The lower limit arises from the requirement that a kick counteracts the SN mass loss and leaves the post-SN system in a tight orbit with a sufficiently small eccentricity; the upper limit arises from the requirement that the binary remains bound. Here we find that, for a given radial velocity, the magnitude of the kick velocity is much better constrained: typically to an interval that is about $\simeq 500 \text{ km s}^{-1}$ wide. If the parameter space is restricted to kinematic ages close to 100 Myr, as in Paper I, the range of allowed kick-velocity magnitudes furthermore narrows from $60 \text{ km s}^{-1} \lesssim V_r \lesssim 1560 \text{ km s}^{-1}$ to $60 \text{ km s}^{-1} \lesssim V_r \lesssim 710 \text{ km s}^{-1}$ for case A disk crossings and to $60 \text{ km s}^{-1} \lesssim V_r \lesssim 850 \text{ km s}^{-1}$ for case B disk crossings. In addition, the kick velocity is smallest when V_r is small and increases with increasing absolute values of V_r (see also Wex et al. 2000). Since the post-SN peculiar velocity V_{pec} generally increases with increasing absolute values of V_r (see Fig. 5), this behavior is consistent with Eq. (8). The highest kick velocities furthermore tend to be associated with the youngest ages.

For case A, we find an absolute lower limit on the kick velocity imparted to pulsar B of $\simeq 60 \text{ km s}^{-1}$ and an absolute upper limit of $\simeq 1660 \text{ km s}^{-1}$; while for case B the absolute lower and upper limits are $\simeq 60 \text{ km s}^{-1}$ and $\simeq 1390 \text{ km s}^{-1}$. The lower limits are in agreement with the lower limit derived in Paper I and with the lower limit derived by Dewi & van den Heuvel (2004). This confor-

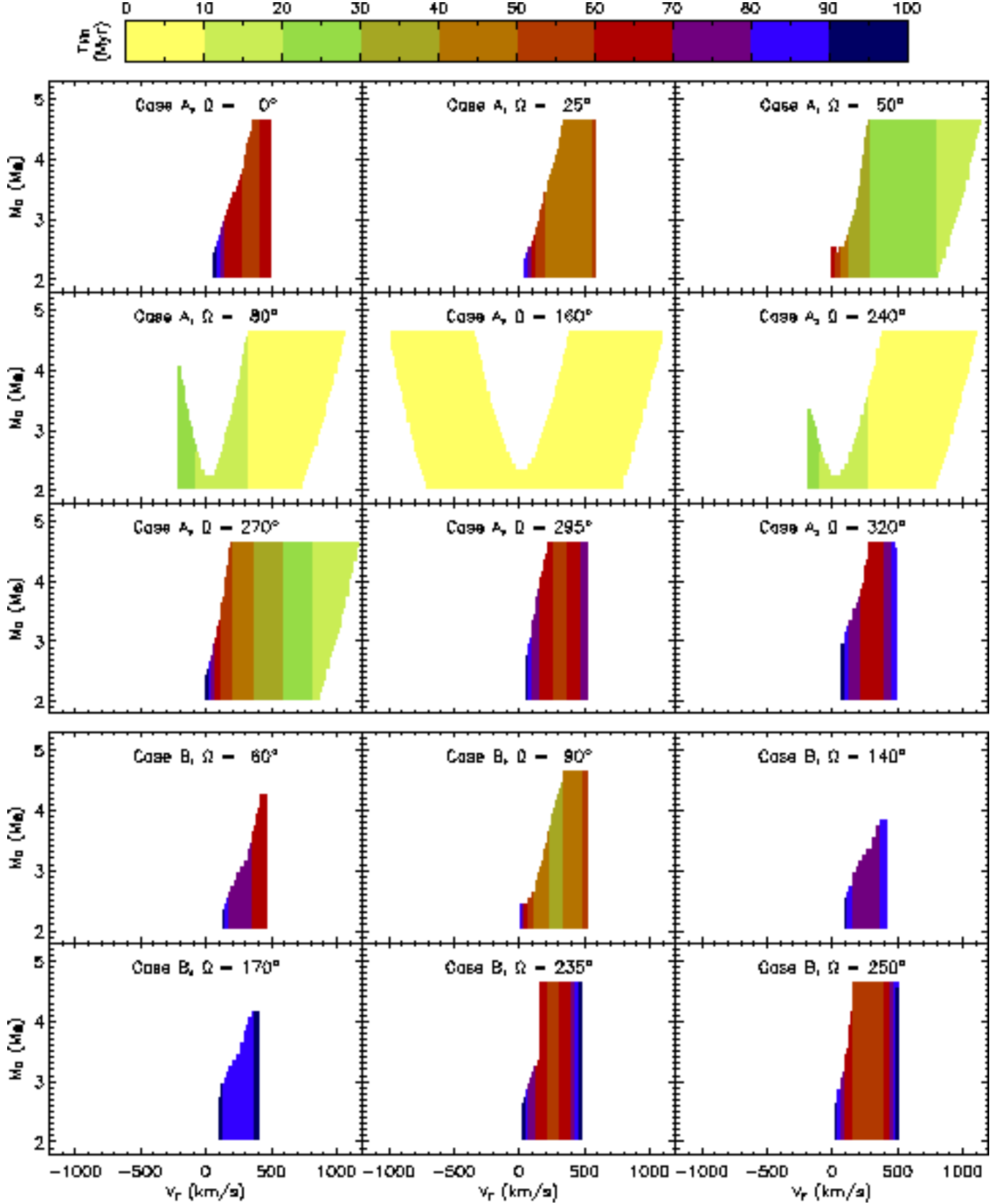


FIG. 6.— Limits on the mass M_0 of PSR J0737-3039B's pre-SN helium star progenitor as a function of V_r , for various values of Ω which were chosen as to provide the clearest and most informative graphical representation. The upper 9 panels are for case A; the lower 6 panels for case B. The gray scale (color in the electronic edition) indicates the kinematic ages associated with different combinations of Ω and V_r (cf. Fig. 3).

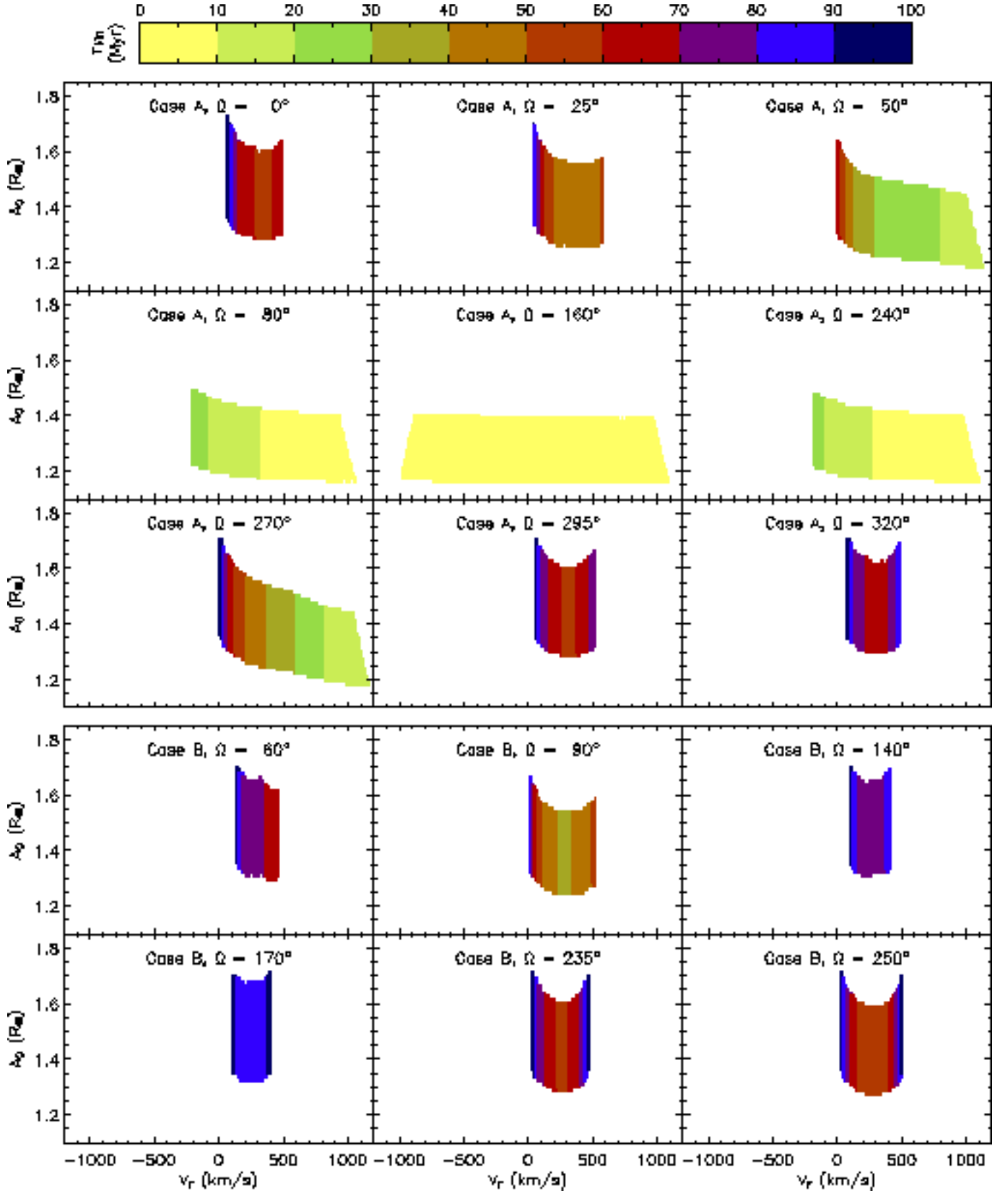


FIG. 7.— Limits on the pre-SN orbital separation A_0 of PSR J0737-3039 as a function of V_r , for various values of Ω . The upper 9 panels are for case A; the lower 6 panels for case B. The gray scale (color in the electronic edition) indicates the kinematic ages associated with different combinations of Ω and V_r (cf. Fig. 3).

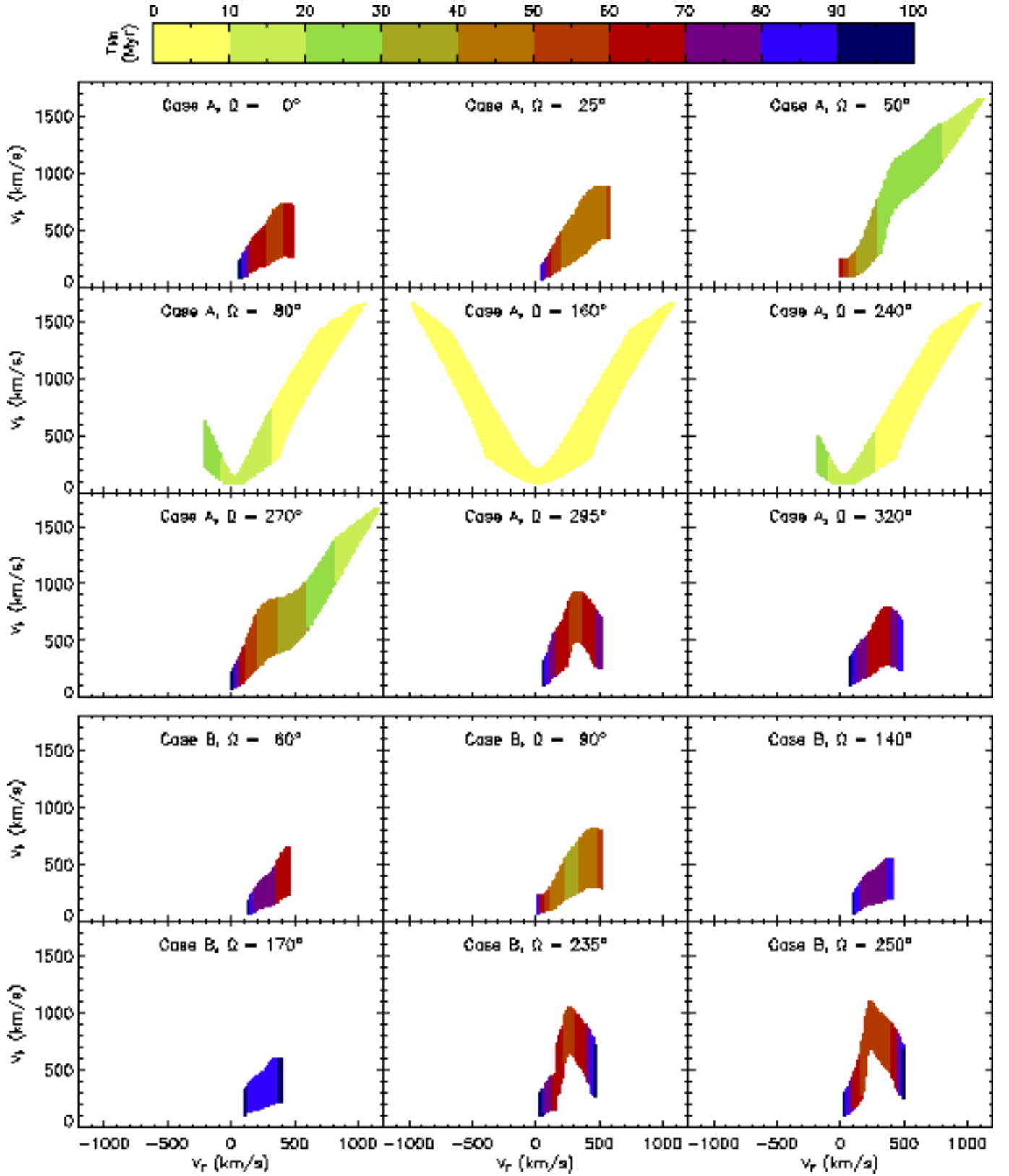


FIG. 8.— Limits on the magnitude V_k of the kick velocity imparted to PSR J0737-3039B at its formation as a function of V_r , for various values of Ω . The upper 9 panels are for case A; the lower 6 panels for case B. The gray scale (color in the electronic edition) indicates the kinematic ages associated with different combinations of Ω and V_r (cf. Fig. 3).

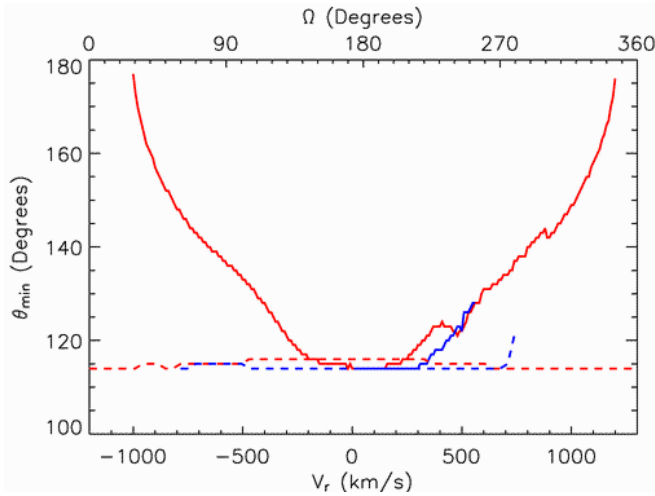


FIG. 9.— Minimum value of the polar angle θ between the pre-SN orbital velocity and the kick velocity imparted to PSR J0737-3039B at its formation as a function of V_r (solid lines, bottom axis) and Ω (dashed lines, top axis). Case A and B are represented by black and light gray lines (red and blue in the electronic edition), respectively.

mity arises because of the moderate post-SN peculiar velocities associated with the Galactic disk crossings found for $|V_r| \lesssim 100 \text{ km s}^{-1}$ (see Fig. 5), which impose no additional constraints on the system in comparison to those already imposed in Paper I. Higher absolute values of the radial velocity would impose additional constraints and shift the minimum kick velocity to higher values. Ransom et al. (2004) furthermore derived a minimum kick velocity of 105 km s^{-1} by assuming that the scintillation velocity component V^\perp of the *current* systemic velocity is entirely due to the kick imparted to the second-born NS (i.e., that the post-SN peculiar velocity is unaffected by the motion in the Galaxy). If we adopt a value of $V^\perp = 90 \text{ km s}^{-1}$, corresponding to the lowest post-SN peculiar velocities found from the Galactic motion calculations (see Fig. 5), in conjunction with an upper limit of $4.7 M_\odot$ on the mass of pulsar B's helium star progenitor, the procedure adopted by Ransom et al. (2004) yields a minimum kick velocity of 75 km s^{-1} . This value is in close agreement with the minimum kick velocity derived above.

The upper limits derived for the magnitude of the kick velocity are determined by the condition that the binary must remain bound after the SN explosion. The condition is expressed by the inequality

$$V_k \leq \left[\frac{G(M_A + M_0)}{A_0} \right]^{1/2} \left[1 + \left(2 \frac{M_A + M_B}{M_A + M_0} \right)^{1/2} \right] \quad (9)$$

(e.g. Brandt & Podsiadlowski 1995, Kalogera & Lorimer 2000). For a given set of NS masses M_A and M_B , the upper limit increases with increasing values of M_0 and with decreasing values of A_0 . Since the absolute lower limit on A_0 derived here is somewhat lower than in Paper I, the absolute upper limit of $\simeq 1660 \text{ km s}^{-1}$ (case A) on V_k is somewhat larger.

The constraints on the direction of the kick velocity imparted to pulsar B at birth are illustrated in Fig. 9, where we show the minimum value θ_{min} of the angle θ between the kick velocity and the helium star's pre-SN

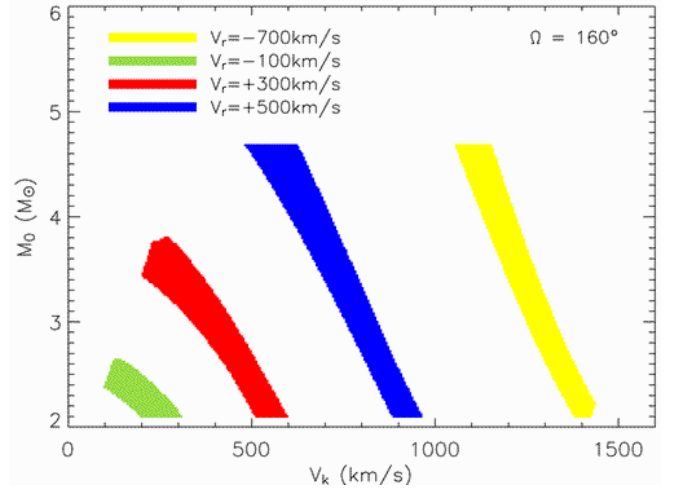


FIG. 10.— Correlations between the mass M_0 of PSR J0737-3039B's pre-SN helium star progenitor and the kick velocity V_k imparted to its center-of-mass at the time of its formation, for case A and $\Omega = 160^\circ$. The different gray shades (colors in the electronic edition) correspond to different values of V_r .

orbital velocity for which all the imposed constraints may be satisfied³. The solid lines show the values of θ_{min} as a function of V_r , while the dashed lines show the values of θ_{min} as a function of Ω . Case A and case B are distinguished by black and light gray lines (red and blue in the electronic edition), respectively. The values of θ_{min} are fairly insensitive to the value of Ω . The dependency on V_r , on the other hand, is much stronger: θ_{min} reaches a minimum value of $\simeq 115^\circ$ for $|V_r| \lesssim 200 \text{ km s}^{-1}$ and then increases with increasing absolute values of V_r . The tendency of the kicks to be directed opposite to the orbital motion therefore becomes stronger with increasing absolute values of the radial velocity (and thus with increasing values of the kick velocity, see Fig. 8).

It is also interesting to examine how the constraints on the helium-star mass M_0 and kick magnitude V_k correlate. For both cases A and B, all pairs of Ω and V_r yield results qualitatively similar to the ones illustrated in Fig. 10. It is evident that, for a given radial velocity, higher masses correlate with lower kicks. This is consistent with our expectations, since stronger SN mass loss requires a smaller kick to achieve the same effect (satisfying all of the constraints). Also as expected, as the absolute value of V_r increases, the constrained band shifts to higher and higher kick magnitudes. Finally, we note that these correlations are derived based on the constraints relevant to the formation of PSR J0737-3039 and do not necessarily reflect a correlation inherent to the kick mechanism. However, a slope for this unknown correlation (because of the physical origin of the kick) similar to the one shown in Fig. 10 would require minimal fine-tuning of parameters for the formation of PSR J0737-3039, and hence would be favored statistically.

2.4. Isotropic Kick Probability Distribution

In Paper I, we derived a probability distribution for the magnitude of the kick velocity imparted to pul-

³ The maximum possible value of θ is usually close to 180° so that no additional constraints arise from considering θ_{max} .

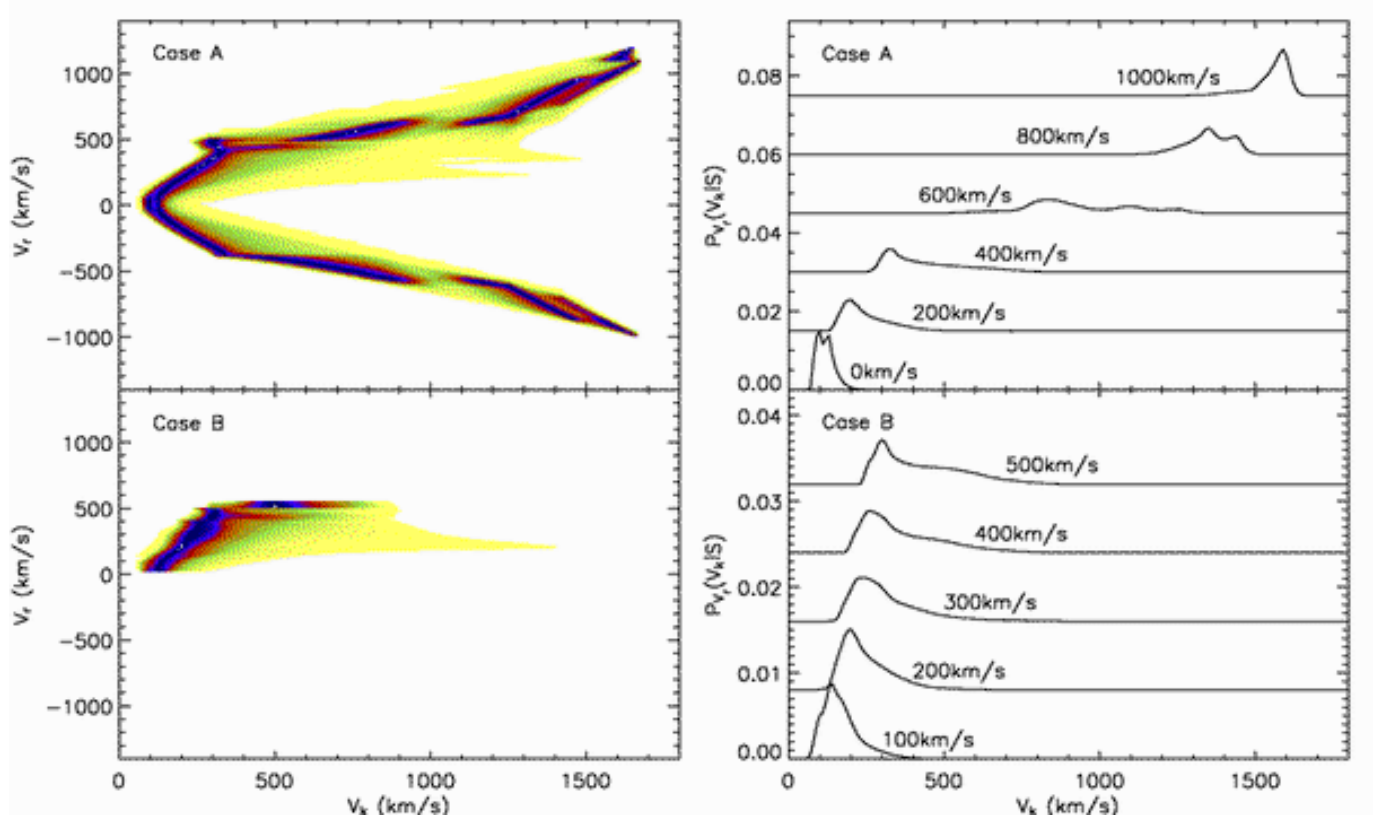


FIG. 11.— Probability distribution functions for the magnitude of the kick velocity imparted to PSR J0737-3039B at the time of its formation, for case A (top panels) and B (bottom panels). The left-hand panels show the entire set of PDFs associated with all admissible V_r -values by means of a linear color scale which varies from light to dark gray with increasing PDF-values (in the electronic edition increasing PDF values are indicated by yellow, green, orange, red, and blue), while the right-hand panels show the PDFs associated with some specific V_r -values. For clarity, the curves in the right-hand panels are offset from each other by an arbitrary amount.

sar B, under the assumption that all kick directions are equally probable. Here, we adopt the same assumption and derive such probability distributions for each combination of Ω and V_r leading to plausible progenitors of PSR J0737-3039. As mentioned before, for either case A or B, each pair (Ω, V_r) determines the kinematic age and hence the post-SN orbital parameters (A, e) . Furthermore, for a given kick-velocity magnitude V_k , a pair of kick-orientation angles (θ, ϕ) corresponds to a finite set of pre-SN properties (M_0, A_0) . Therefore, for each pair of (Ω, V_r) and for a given value of V_k , we can calculate the likelihood of a pair (θ, ϕ) that satisfies the M_0, A_0 constraints as

$$\begin{aligned} \Lambda_{V_r, \Omega}(\theta, \phi | V_k) &\equiv \Lambda(\theta, \phi | V_k, V_r, \Omega) \\ &= \frac{j}{2\pi} \frac{\sin \theta}{2}, \text{ if } M_0(\theta, \phi) \text{ and } A_0(\theta, \phi) \\ &\quad \text{satisfy the constraints} \\ &= 0, \quad \text{if not,} \end{aligned} \quad (10)$$

where the polar angle θ is determined by Eq. (6), and j denotes the number of allowed (M_0, A_0) solutions associated with (θ, ϕ) for the considered V_k .

Using Bayes' theorem, the likelihood in Eq. (10) is transformed into a probability that, for a given pre-SN orbital separation A_0 and helium-star mass M_0 , the kick-velocity imparted to pulsar B had a magnitude V_k :

$$P_{V_r, \Omega}(V_k | \theta, \phi)$$

$$= \frac{P_{V_r, \Omega}(V_k) \Lambda_{V_r, \Omega}(\theta, \phi | V_k)}{\int_0^\infty \Lambda_{V_r, \Omega}(\theta, \phi | V'_k) P_{V_r, \Omega}(V'_k) dV'_k} \quad (11)$$

(e.g. Bevington & Robinson 2002). Here $P_{V_r, \Omega}(V_k)$ is the probability that, for a given V_r and Ω , the kick velocity had a magnitude V_k when no particular set of pre- and post-SN binary parameters is imposed. Since, in this case, there is no reason to favor any kick-velocity magnitude over another, we set $P_{V_r, \Omega}(V_k) = 1$.

The total probability that the kick velocity imparted to pulsar B had a magnitude V_k is obtained by deriving a distribution function $P_{V_r, \Omega}(V_k | \theta, \phi)$ for each admissible (A_0, M_0) pair and performing the integration

$$P_{V_r, \Omega}(V_k | S) = \int_S P_{V_r, \Omega}(V_k | \theta, \phi) d\theta d\phi. \quad (12)$$

Here, S denotes the region of (θ, ϕ) -values corresponding to the entire region of admissible A_0 - and M_0 - values in the constrained (A_0, M_0) -parameter space.

To obtain a set of kick-velocity distributions associated with different values of V_r , finally, we assume the longitude of the ascending node to be uniformly distributed in the plane perpendicular to the line-of-sight, and integrate the distribution functions $P_{V_r, \Omega}(V_k | S)$ over all possible values of Ω :

$$P_{V_r}(V_k | S) = \frac{1}{2\pi} \int_0^{2\pi} P_{V_r, \Omega}(V_k | S) d\Omega. \quad (13)$$

The probability distribution functions $P_{V_r}(V_k | S)$ are displayed in the left-hand panels of Fig. 11 by means

of a linear color scale varying from light to dark gray with increasing PDF-values (in the electronic edition increasing PDF values are indicated by yellow, green, orange, red, and blue). We stress that the figure depicts a set of individual one-dimensional kick-velocity distributions associated with different V_r -values, and not a single two-dimensional distribution function of V_k and V_r . The right-hand panels of the figure show the probability distribution functions (PDFs) associated with some specific values of V_r .

For case A disk crossings, the majority of the distributions peak at a *single* value of V_k , which increases with increasing absolute values of V_r (cf. Fig. 8). This single-peaked behaviour is in contrast to the behaviour found in Paper I, where the kick-velocity distribution showed a primary peak around 150 km s^{-1} , and a smaller secondary peak at $\simeq 1200\text{--}1300 \text{ km s}^{-1}$. The disappearance of the double-peaked structure is associated with the additional constraints imposed by the post-SN peculiar velocities derived from the Galactic motion calculations: since kick velocities of the order of 150 km s^{-1} give rise to very different post-SN peculiar velocities than kick velocities of the order of $1200\text{--}1300 \text{ km s}^{-1}$, the extra condition effectively eliminates one of the two peaks in favor of the other one. When $|V_r| \lesssim 400 \text{ km s}^{-1}$, the peak in the distribution functions occurs at kick velocities of $\simeq 100\text{--}300 \text{ km s}^{-1}$, while for $|V_r| \gtrsim 1000 \text{ km s}^{-1}$ it occurs at kick velocities in excess of 1500 km s^{-1} . For intermediate values of $|V_r|$ ($\simeq 600\text{--}800 \text{ km s}^{-1}$), a hint of a double-peaked structure is still present, although the two peaks are much more evenly matched in height and occur much closer to each other than those found in paper I.

For case B disk crossings, the distribution functions always show a single-peaked behaviour. The most probable kick velocity again increases with increasing absolute values of V_r and, for $V_r \lesssim 500 \text{ km s}^{-1}$, ranges from approximately 150 km s^{-1} to 300 km s^{-1} . For larger absolute values of the radial velocity, the most probable kick velocity is about $\simeq 500 \text{ km s}^{-1}$, although only few case B disk crossings occur for these high radial velocities.

Since the probability of a given V_k depends on the constraints derived for A_0 and M_0 , we tested the robustness of the distribution functions to some of the assumptions adopted in the previous sections. In particular, we varied the constraints on A_0 by considering both a lower upper limit of 50 Myr and a higher upper limit of 150 Myr on the age of the system⁴. We find that neither the lower nor the higher age yields significant changes in the distribution functions, so that our results are insensitive to reasonable changes in the constraints derived for A_0 . In addition, the lower limit of $2.1 M_\odot$ on the mass M_0 of pulsar B's helium star progenitor was determined by the lowest mass for which a *non-Roche-lobe-filling* helium star is expected to form a NS. However, since the pre-SN system is most likely undergoing a mass-transfer phase which was initiated after the cessation of core helium burning, the lower limit of $2.1 M_\odot$ should actually be applied to the mass of the helium star at the onset of Roche-lobe overflow. The mass M_0 at the time of the second SN explosion may then actually be somewhat lower than $2.1 M_\odot$. We have

⁴ Recall that the age affects the range of possible A_0 -values through the constraint $A(1 - e) \leq A_0 \leq A(1 + e)$, where A and e are the post-SN orbital parameters.

therefore reconsidered the derivation of the distribution functions for a lower limit on M_0 of $1.4 M_\odot$ and did not find any significant changes in the PDFs. The reason for this is twofold. Firstly, the increase in the admissible (A_0, M_0) -parameter space resulting from a decrease of the lower limit on M_0 is small in comparison to the total size of the parameter space. A decrease in the minimum kick velocity associated with a decrease in the minimum helium star mass (cf. Paper I) therefore has a very low weight in the construction of the PDFs. Secondly, for $M_0 \lesssim 1.8 M_\odot$ the minimum kick velocity is no longer determined by the lower limit on M_0 but by the constraints on the post-SN peculiar velocity V_{pec} . This is readily seen from Eq. (8) when one uses the inequalities $V_{\text{pec}} \gtrsim 90 \text{ km s}^{-1}$, $A_0 \lesssim 1.72 R_\odot$, and $A \lesssim 1.54 R_\odot$. Finally, the upper limit on M_0 was varied by considering different critical mass ratios separating dynamically stable from dynamically unstable Roche-lobe overflow. The behavior of the PDFs again did not show any significant changes.

2.5. Tilt Probability Distributions

According to our current understanding of the formation of DNS binaries, the mass-transfer phase responsible for spinning up pulsar A to millisecond periods is also expected to align pulsar A's spin-axis with the pre-SN orbital angular momentum axis. Depending on its magnitude and orientation, the SN kick imparted to pulsar B at the time of its formation may tilt the post-SN orbit with respect to the pre-SN orbital plane, thus causing a misalignment between pulsar A's spin axis and the post-SN orbital angular momentum axis. The tilt angle λ is related to the pre- and post-SN binary parameters and to the magnitude and direction of the kick velocity as

$$\cos \lambda = \left[\frac{A}{A_0} \frac{M_A + M_B}{M_A + M_0} (1 - e^2) \right]^{-1/2} \times \left(\frac{V_k}{V_0} \cos \theta + 1 \right) \quad (14)$$

(Kalogera 2000). The dependence of the tilt angle on the direction of the kick velocity is thus entirely through the polar angle θ with no contribution whatsoever from the azimuthal angle ϕ .

In order to derive a set of probability distribution functions $P_{V_r}(\lambda|S)$ for the tilt angle λ , we use Eq. (14) to eliminate V_k from Eqs. (6) and (7). After the elimination, the derivation of the distribution functions is similar to the derivation of the kick-velocity distributions $P_{V_r}(V_k|S)$ outlined in Section 2.4. The resulting PDFs are presented in Fig. 12 in a similar fashion as the kick-velocity distributions shown in Fig. 11.

For case A disk crossings, the tilt-angle distributions generally show a single peak which becomes wider and moves to larger tilt angles with increasing absolute values of V_r . For $|V_r| \lesssim 400 \text{ km s}^{-1}$, the peak occurs at tilt angles $\lambda \lesssim 30^\circ$; while for $|V_r| \gtrsim 1000 \text{ km s}^{-1}$ it occurs at $\lambda \gtrsim 135^\circ$ although it becomes much less pronounced. For intermediate V_r -values ($\simeq 600 \text{ km s}^{-1}$), a hint of a double-peaked structure is present. Tilt angles close to $\lambda \approx 90^\circ$ are furthermore strongly disfavored regardless of the value of the radial velocity because they require greatly fine-tuned kick magnitudes and directions satisfying $V_k \cos \theta \approx -V_0$ (see Eq. 14). Case B disk cross-

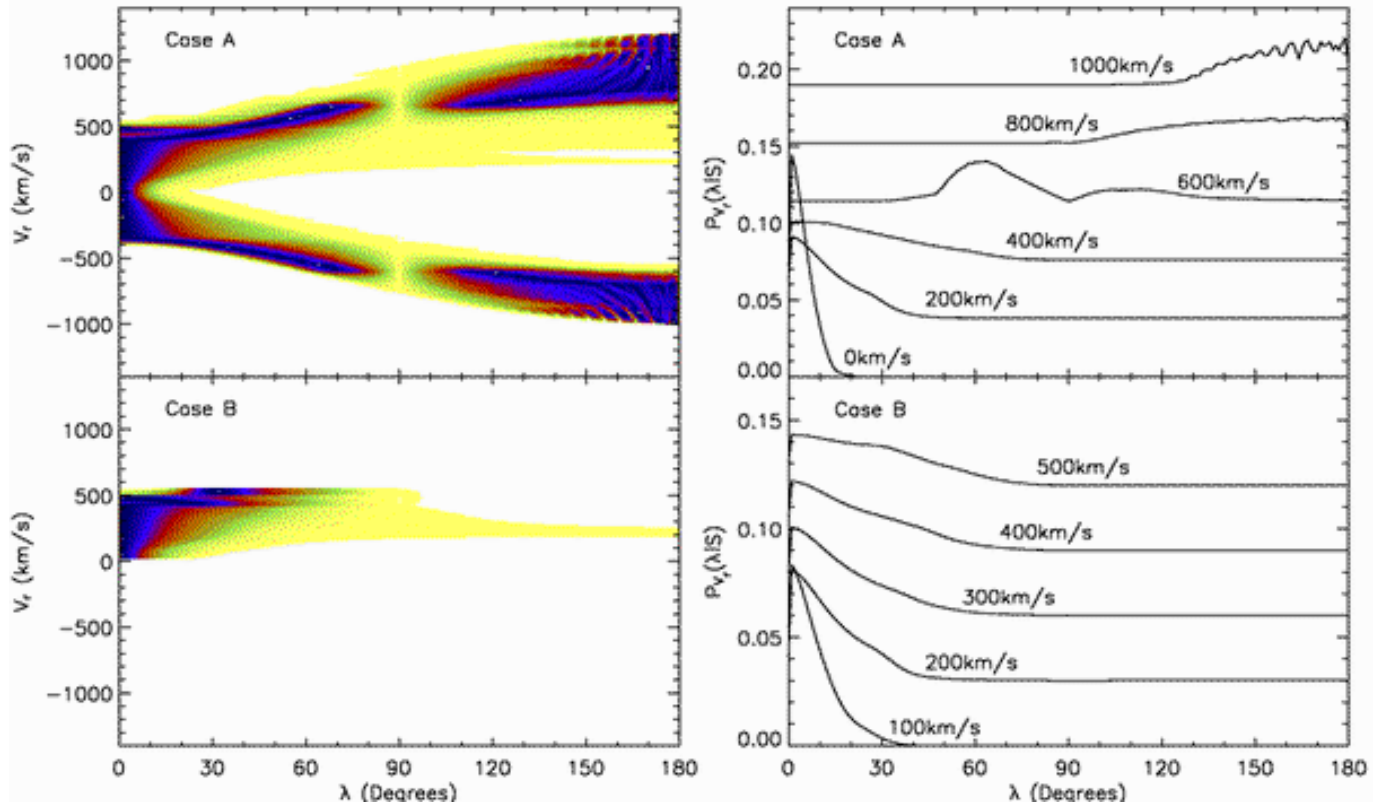


FIG. 12.— Probability distribution functions for the misalignment angle λ between PSR J0737-3039A’s spin axis and the post-SN orbital angular momentum axis, for case A and B. The left-hand panels show the entire set of PDFs associated with all admissible V_r -values by means of a linear color scale which varies from light to dark gray with increasing PDF-values (in the electronic edition increasing PDF values are indicated by yellow, green, orange, red, and blue), while the right-hand panels show the PDFs associated with some specific V_r -values. For clarity, the curves in the right-hand panels are offset from each other by an arbitrary amount.

ings, on the other hand, yield distributions which typically peak at tilt angles $\lambda \lesssim 30^\circ$. The peak is most pronounced when $V_r \lesssim 400 \text{ km s}^{-1}$ and flattens somewhat for $V_r \gtrsim 400 \text{ km s}^{-1}$. In the latter case, the distributions still favor tilt angles below 70° . As for the kick-velocity distributions, these results are very insensitive to the assumptions adopted in the derivation of the A_0 - and M_0 -constraints, for both case A and case B. The overall behavior of the tilt-probability distributions is furthermore in excellent agreement with the analytical spin-tilt distributions in coalescing binaries with two compact objects derived by Kalogera (2000).

We conclude this section by noting that the geometrical model constructed by Jenet & Ransom (2004) to explain the flux variations of PSR J0737-3039B predicts tilt angles of $16^\circ \pm 10^\circ$ or $164^\circ \pm 10^\circ$. The PDFs presented in Fig. 12 favor the lower tilt angle when $|V_r| \lesssim 400 \text{ km s}^{-1}$ and the higher tilt angle when $|V_r| \gtrsim 800 \text{ km s}^{-1}$. The alternative solutions of $82^\circ \pm 16^\circ$ or $98^\circ \pm 16^\circ$ derived by Jenet & Ransom (2004) are strongly disfavored by all distribution functions. As noted by the authors, these solutions are also incompatible with the misalignment angle between the pulsar’s spin and magnetic dipole axes derived by Demorest et al. (2004).

2.6. Non-isotropic kicks

The probability distribution functions for the kick-velocity magnitude V_k and the spin misalignment angle λ

presented in the previous sections were derived under the assumption that all kick directions are equally probable. However, in recent years a possible alignment of the SN kick with the NS spin axis has been discussed, prompted mainly by the alignment of pulsar proper motion vectors with jet axes in the Crab and the Vela pulsars (Lai, Chernoff, & Cordes 2001; Romani 2004).

Assuming that the NS spin axis is determined by the axis of the progenitor helium star and that this axis was roughly aligned with the pre-SN orbital angular momentum axis due to mass transfer, the alignment inferred by these observations possibly indicates a preference for kick directions perpendicular to the pre-SN orbital plane. In order to examine the effect of such preferred kick directions, we reconsider the derivation of the kick-velocity and tilt-angle distributions under the assumption that the kick direction is restricted to be within two oppositely directed cones with opening angle ξ_p and with axes parallel to the pre-SN orbital angular momentum axis (i.e., polar kicks). For this purpose, it is convenient to introduce the angle $\xi \in [0, \pi]$ between the kick-velocity vector and the pre-SN orbital angular momentum vector as a measure for the spin-kick alignment. The angle is related to the kick-direction angles θ and ϕ by the equation

$$\cos \xi = \sin \theta \cos \phi, \quad (15)$$

so that kicks are directed within the above mentioned cones with opening angle ξ_p when

$$\cos \xi_p \leq |\sin \theta \cos \phi| \leq 1 \quad (16)$$

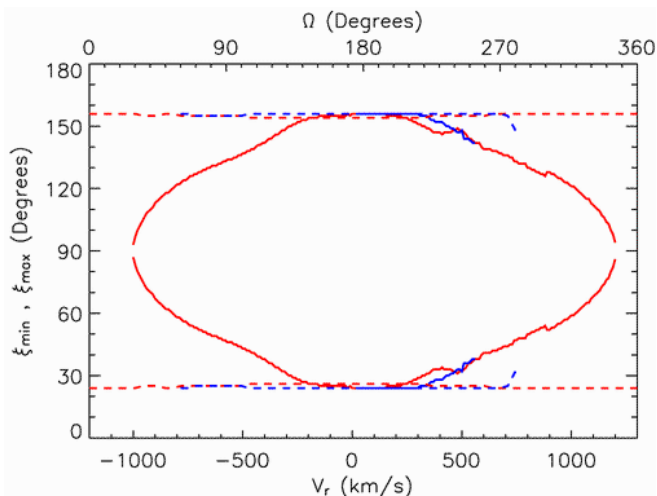


FIG. 13.— Limits on the polar angle ξ between the pre-SN orbital angular momentum axis and the kick velocity imparted to PSR J0737-3039B at its formation as a function of V_r (solid lines, bottom axis) and Ω (dashed lines, top axis). Values of ξ smaller than 90° are lower limits (ξ_{\min}); values of ξ larger than 90° are upper limits (ξ_{\max}). Case A and B are represented by black and light gray lines (red and blue in the electronic edition), respectively.

(Kalogera 2000). We also note that since, for a given kick-velocity magnitude V_k , four solutions (θ, ϕ) of Eqs. (6) and (7) exist for each set of admissible pre- and post-SN binary parameters, there is also a two-fold degeneracy in the solutions for ξ .

The range of ξ angles available for the formation of PSR J0737-3039 is shown in Fig. 13 as a function of V_r and Ω . Curves below 90° correspond to lower limits, ξ_{\min} , and curves above 90° to upper limits, ξ_{\max} . Case A and B are indicated by black and light gray lines (red and blue in the electronic edition), respectively. It is interesting to note that it would be impossible to understand the formation of PSR J0737-3039, if the kick were very closely aligned or anti-aligned to the pre-SN orbital angular momentum (that could also determine the newborn NS spin). Instead a minimum deviation from the pre-SN orbital angular momentum axis of 25° – 30° appears to be necessary to satisfy all the imposed constraints.

In order to illustrate the effects of polar kicks, we considered the case where $\xi_p = 30^\circ$. The reduction in the available parameter space associated with the restriction of the kick direction yields viable solutions for case A only when $|V_r| \lesssim 300 \text{ km s}^{-1}$, and for case B only when $0 \text{ km s}^{-1} \lesssim V_r \lesssim 500 \text{ km s}^{-1}$. In addition, the mass of pulsar B's helium star progenitor becomes constrained to $M_0 \approx 2.1$ – $2.5 M_\odot$, the pre-SN orbital separation to $A_0 \approx 1.1$ – $1.5 R_\odot$, and the magnitude of the kick velocity to $V_k \approx 100$ – 600 km s^{-1} .

In Figs. 14 and 15, we show the kick-velocity and tilt-angle distribution functions in the case of polar kicks with $\xi_p = 30^\circ$. Both sets of distributions clearly show a much more pronounced single peak than when the kicks are assumed to be distributed isotropically (cf. Figs. 11 and 12). Depending on the radial velocity, the most probable kick velocity ranges from approximately 200 km s^{-1} to 550 km s^{-1} , and the most probable tilt angle from 15° to 45° . This range of tilt angles is compatible with the tilt angle of $16^\circ \pm 10^\circ$ predicted by Jenet & Ransom

(2004).

3. THE RECENT EVOLUTIONARY HISTORY OF PSR B1534+12

Unlike PSR J0737-3039, the relativistic binary radio pulsar PSR B1534+12 has an accurately measured proper motion with a known direction in right ascension and declination (see Table 1), so that its kinematic history and progenitor constraints *depend only on the unknown radial velocity* V_r . In order to derive these constraints, we adopt the spin-down age $\tau_b = 210 \text{ Myr}$ as an upper limit to the age of the system. The other physical parameters of PSR B1534+12 relevant to the derivation are summarised in Table 1.

Following the same arguments as for PSR J0737-3039 in Section 2.2, we assume that PSR B1534+12 was close to the Galactic plane at the time of the second SN explosion and that its pre-SN systemic velocity was almost entirely due to Galactic rotation. The possible birth sites of the DNS are then obtained by tracing the Galactic motion of the system backwards in time as a function of the unknown radial velocity V_r . We find that, within the imposed age limit of 210 Myr , no Galactic plane crossings occur when $V_r \lesssim -280 \text{ km s}^{-1}$, whereas up to four crossings may occur when $V_r \gtrsim -280 \text{ km s}^{-1}$. Since four disk crossings only occur for relatively few and rather fine-tuned Galactic trajectories, we leave these cases aside and focus on the possible birth sites associated with the first (case A), second (case B), and third (case C) Galactic plane crossings.

The kinematic ages and post-SN peculiar velocities associated with the Galactic plane crossings are shown in Fig. 16 as functions of the radial velocity V_r . Case A gives rise to a wide range of ages between $\simeq 1 \text{ Myr}$ and 210 Myr , and peculiar velocities between 80 km s^{-1} and 1500 km s^{-1} . Cases B and C, on the other hand, yield kinematic ages of *at least* $\simeq 90 \text{ Myr}$ and $\simeq 130 \text{ Myr}$; and post-SN peculiar velocities of 100 – 220 km s^{-1} and 80 – 160 km s^{-1} , respectively.

The post-SN orbital separation A and orbital eccentricity e at the times of Galactic disk crossings are obtained by numerical integration backwards in time of the equations governing the evolution of the orbit under the influence of gravitational radiation. The resulting post-SN orbital parameters range from $A = 3.28 R_\odot$ and $e = 0.274$ when $\tau_{\text{kin}} = 0 \text{ Myr}$ to $A = 3.36 R_\odot$ and $e = 0.282$ when $\tau_{\text{kin}} = 210 \text{ Myr}$. These post-SN orbital parameters together with the post-SN peculiar velocities impose constraints on the pre-SN progenitor of PSR B1534+12. These are derived in a similar way as for the progenitor of PSR J0737-3037 (except that the problem depends on only one free parameter, V_r). The results of our analysis are summarized in Fig. 17.

Contrary to PSR J0737-3039, which was most likely in a state of mass transfer just before the second SN explosion, PSR B1534+12 may have been detached as well as semi-detached at the time the second NS was born. In order to illustrate this, the solutions for which no mass transfer takes place at the time of the second SN explosion are indicated by the dark gray (red in the electronic edition) regions in Fig. 17, while the light gray (blue in the electronic edition) regions indicates the *additional* solutions that become accessible when the possibility of mass transfer is taken into account. For the latter solu-

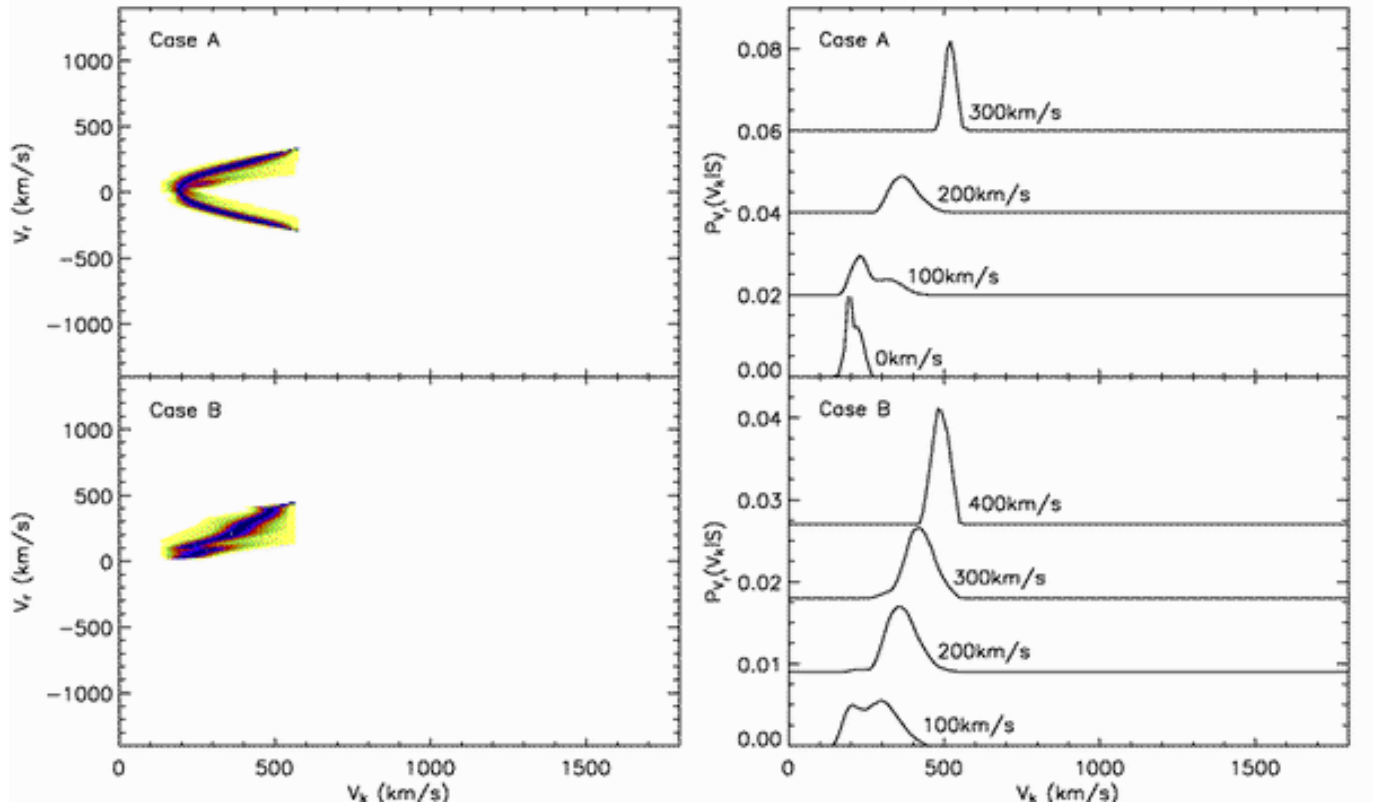


FIG. 14.— Probability distribution functions for the magnitude V_k of the kick velocity imparted to PSR J0737-3039B at the time of its formation, for polar kicks restricted to two oppositely directed cones with an opening angle of $\xi_p = 30^\circ$ and with axes parallel to the pre-SN orbital angular momentum axis (cf. Fig. 11 for more details).

tions we adopt the same assumption as before that the system may survive the mass transfer phase and form a DNS only if the mass ratio M_0/M_A is smaller than 3.5 (e.g., Ivanova et al. 2003).

For case A disk crossings, detached pre-SN binary configurations exist only for $V_r \gtrsim 250 \text{ km s}^{-1}$. For smaller radial velocities, the system is always undergoing mass transfer from the progenitor of the second-born NS to the first-born NS. The pre-SN mass of the helium star forming the second NS is constrained within $2.1 M_\odot - 8 M_\odot$. The lower limit again corresponds to the lowest mass for which a helium star is expected to form a NS instead of a white dwarf, while the upper limit corresponds to the highest mass for which a helium star is expected to form a NS rather than a black hole (see, e.g., Fig. 1 in Belczynski, Kalogera, & Bulik 2002; and Table 16.4 in Tauris & van den Heuvel 2004). The divide between the dark and light gray (red and blue in the electronic edition) regions at $4.7 M_\odot$ corresponds to the adopted critical mass ratio $M_0/M_A = 3.5$ for dynamically stable mass transfer. The allowed mass range of pre-SN helium star masses is most constrained for $|V_r| \lesssim 200 \text{ km s}^{-1}$ when $2.1 M_\odot \lesssim M_0 \lesssim 4 M_\odot$. Lower and upper limits on the pre-SN orbital separation are given by $2.4 R_\odot$ and $4.3 R_\odot$.

The behavior of the kick-velocity magnitude is similar as for PSR J0737-3039: the kick velocity increases with increasing absolute values of V_r and, for a given radial velocity, it is generally constrained to an interval that is less than $\simeq 600 \text{ km s}^{-1}$ wide. When all possible

pre-SN binary configurations are considered, the kick velocity magnitudes range from 15 km s^{-1} to 1350 km s^{-1} . When configurations for which the helium star is overflowing its Roche lobe are excluded, the range narrows to $230 \text{ km s}^{-1} \lesssim V_k \lesssim 1350 \text{ km s}^{-1}$, so that the minimum kick velocity is higher than when the possibility of Roche-lobe overflow is taken into account. The larger minimum kick velocity is required to compensate the larger effect of the mass lost from the system during the SN explosion: since the minimum M_0 for these systems is $4.7 M_\odot$, at least 57% of the total pre-SN mass is lost from the system. The minimum and maximum kick velocities are furthermore in good agreement with those derived by Fryer & Kalogera (1997) and Dewi & Pols (2003).

The polar angle θ between the kick velocity and the helium star's pre-SN orbital velocity is always larger than 95° , so that the kicks tend to be directed opposite to the orbital motion. When the solutions are restricted to those where no Roche-lobe overflow is going on at the time of the second SN explosion, the direction of the kick velocity is constrained to $\theta \gtrsim 140^\circ$. These values are again in good agreement with those derived by Dewi & Pols (2003). The angle ξ between the kick velocity and the pre-SN orbital angular momentum axis, on the other hand, takes values between 5° and 175° . When the parameter space is restricted to the solutions where the binary is detached just before the second SN explosion, the range of possible ξ -values narrows to $55^\circ \lesssim \xi \lesssim 125^\circ$.

For case B disk crossings, all allowed pre-SN binary configurations imply that the helium star progenitor of

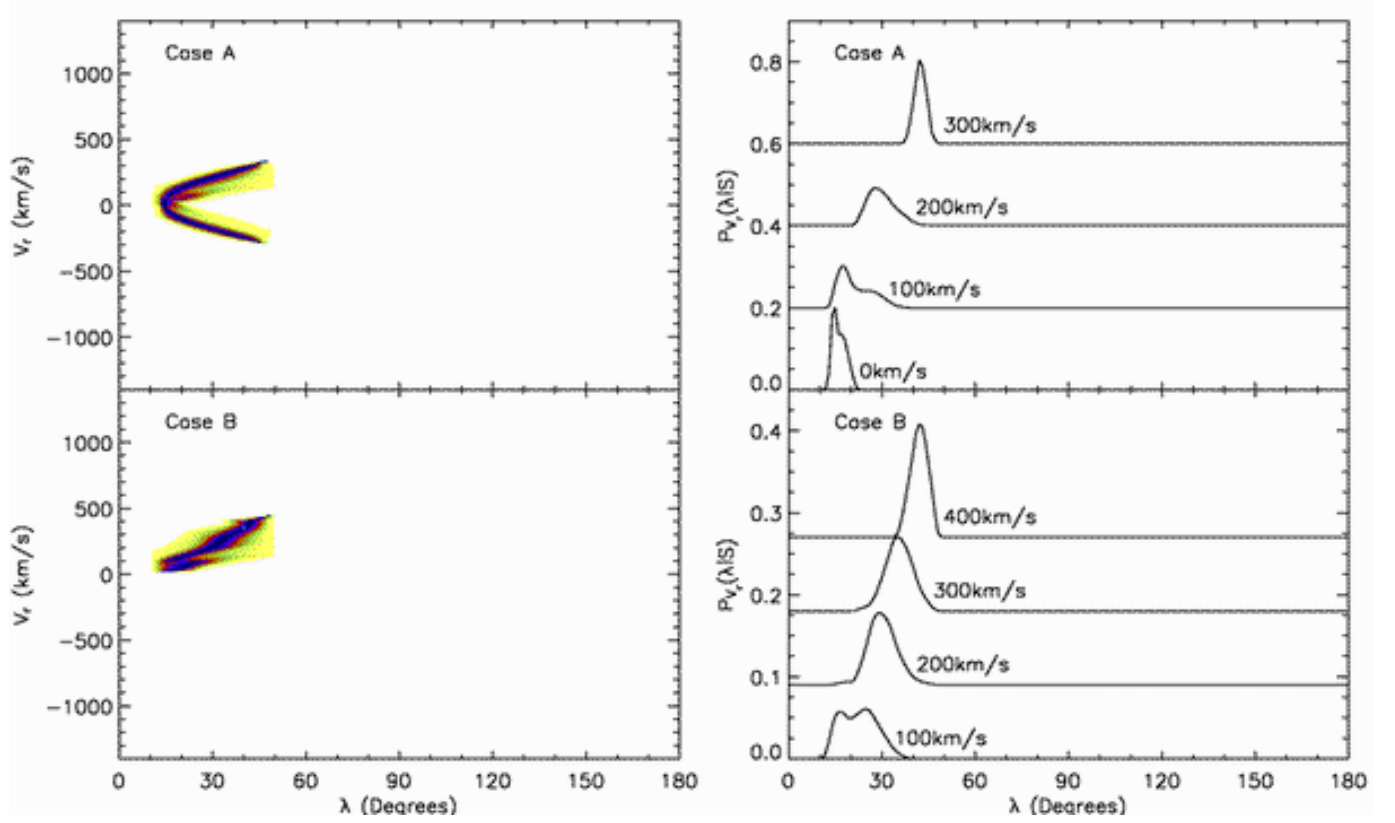


FIG. 15.— Probability distribution functions for the misalignment angle λ between PSR J0737-3039A's spin axis and the post-SN orbital angular momentum axis, for polar kicks restricted to two oppositely directed cones with an opening angle of $\xi_p = 30^\circ$ and with axes parallel to the pre-SN orbital angular momentum axis (cf. Fig. 12 for more details).

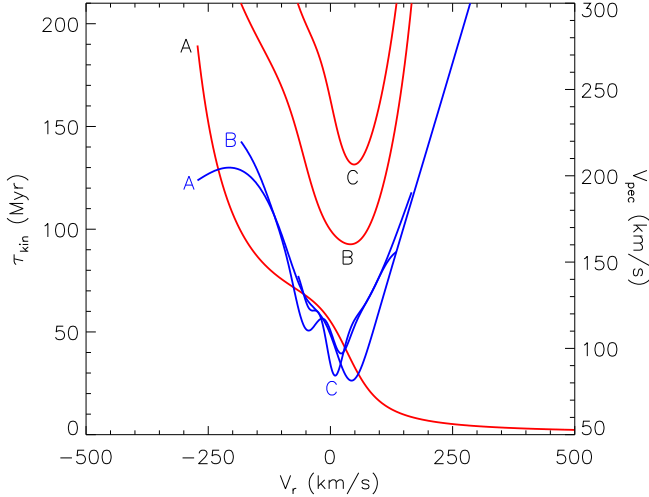


FIG. 16.— Variations of the kinematic age (left-hand axis) and post-SN peculiar velocity (right-hand axis) of PSR B1534+12 as a function of the unknown radial velocity V_r , for cases A, B, and C. The kinematic ages are represented by black solid lines (red in the electronic edition) and the peculiar velocities by light gray lines (blue in the electronic edition).

the second-born NS is overflowing its Roche lobe at the time of its SN explosion. The mass of the helium star is constrained to $2.1 M_\odot \lesssim M_0 \lesssim 4.1 M_\odot$, the pre-SN orbital separation to $2.4 R_\odot \lesssim A_0 \lesssim 4.3 R_\odot$, and the kick-velocity magnitude to $30 \text{ km s}^{-1} \lesssim V_k \lesssim 390 \text{ km s}^{-1}$. The

angle between the kick direction and the helium star's pre-SN orbital velocity is restricted $100^\circ \lesssim \theta \lesssim 180^\circ$, and the angle between the kick direction and the pre-SN orbital angular momentum axis to $10^\circ \lesssim \xi \lesssim 170^\circ$.

Case C disk crossings, finally, also yield no detached solutions for the progenitor of PSR B1534+12. The constraints for this case are similar to those found for case B, except that the mass M_0 is always smaller than $\approx 3.1 M_\odot$ and the kick velocity V_k is always smaller than 270 km s^{-1} .

From these constraints, it follows that, if the case for the alignment of kicks with the spin of the NS's progenitor gets more support in the future, the direct progenitor of PSR B1534+12's companion must be overflowing its Roche lobe, regardless of which disk crossing corresponds to the birth place. In addition, as for PSR J0737-3039, the formation of PSR B1534+12 cannot be explained if the kick imparted to PSR B1534+12's companion was *perfectly* aligned or anti-aligned with the spin of its progenitor.

The constraints derived above may again be used to derive probability distribution functions for the magnitude V_k of the kick velocity imparted to the second-born NS and for the misalignment angle λ between the spin-axis of the first-born NS and the post-SN orbital angular momentum axis (cf. Sections 2.4 and 2.5). The resulting PDFs are presented in Figs. 18 and 19 as those for PSR J0737-3039 in Figs. 11 and 12. For radial velocities of only a few 100 km s^{-1} , the kick-velocity distributions show two closely spaced and fairly evenly matched

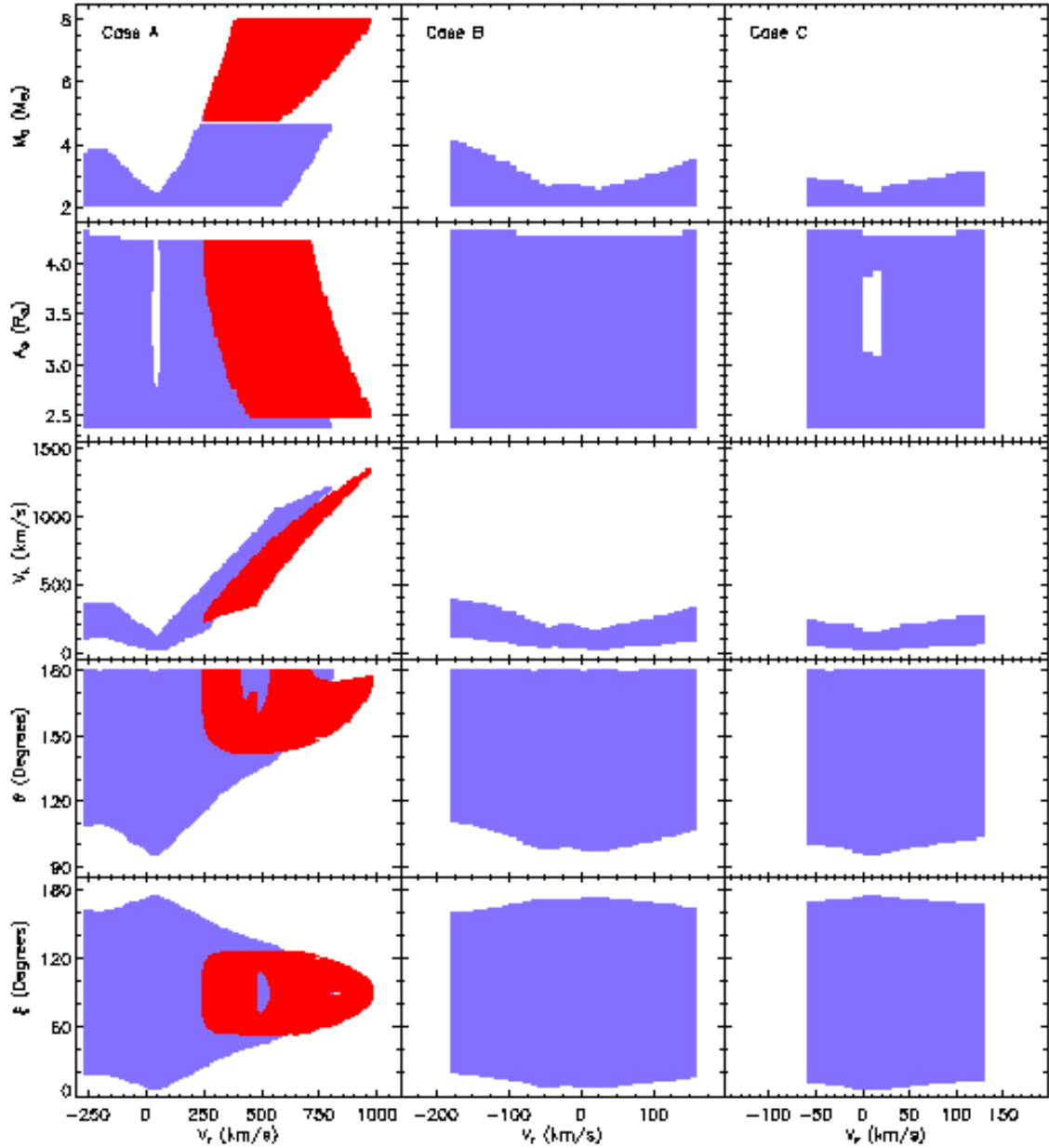


FIG. 17.— Limits on the pre-SN progenitor of PSR B1534+12 and on the kick velocity imparted to the last-born NS. The left-hand panels show the constraints for case A, the middle panels for case B, and the right-hand panels for case C. Dark gray (red in the electronic edition) regions correspond to solutions for which the pre-SN binary is detached, while light gray (blue in the electronic edition) regions indicate the additional solutions associated with mass-transferring systems.

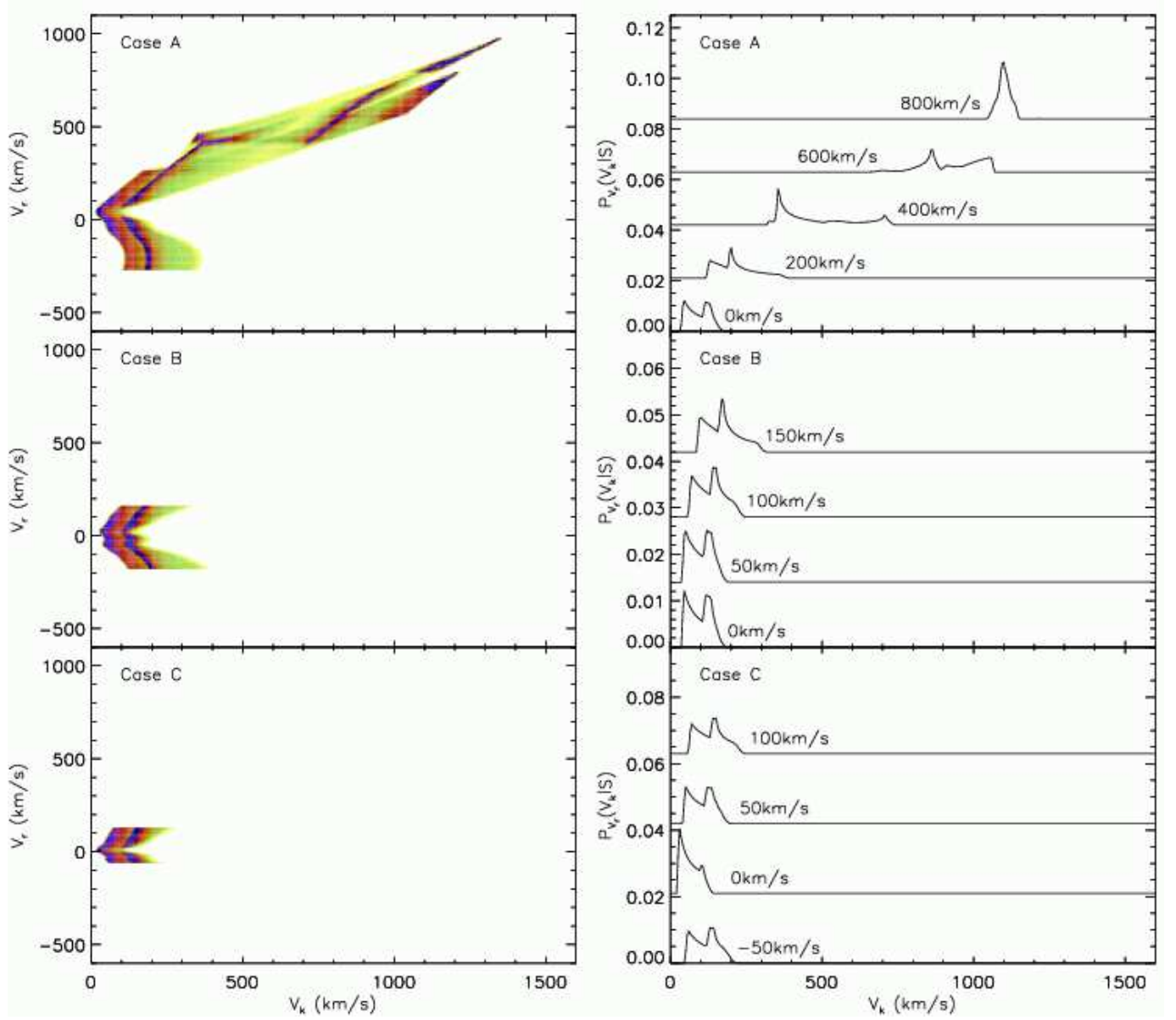


FIG. 18.— Probability distribution functions of the magnitude of the kick velocity imparted to PSR B1534+12's companion at the time of its formation, for cases A, B, and C (cf. Fig. 11 for more details).

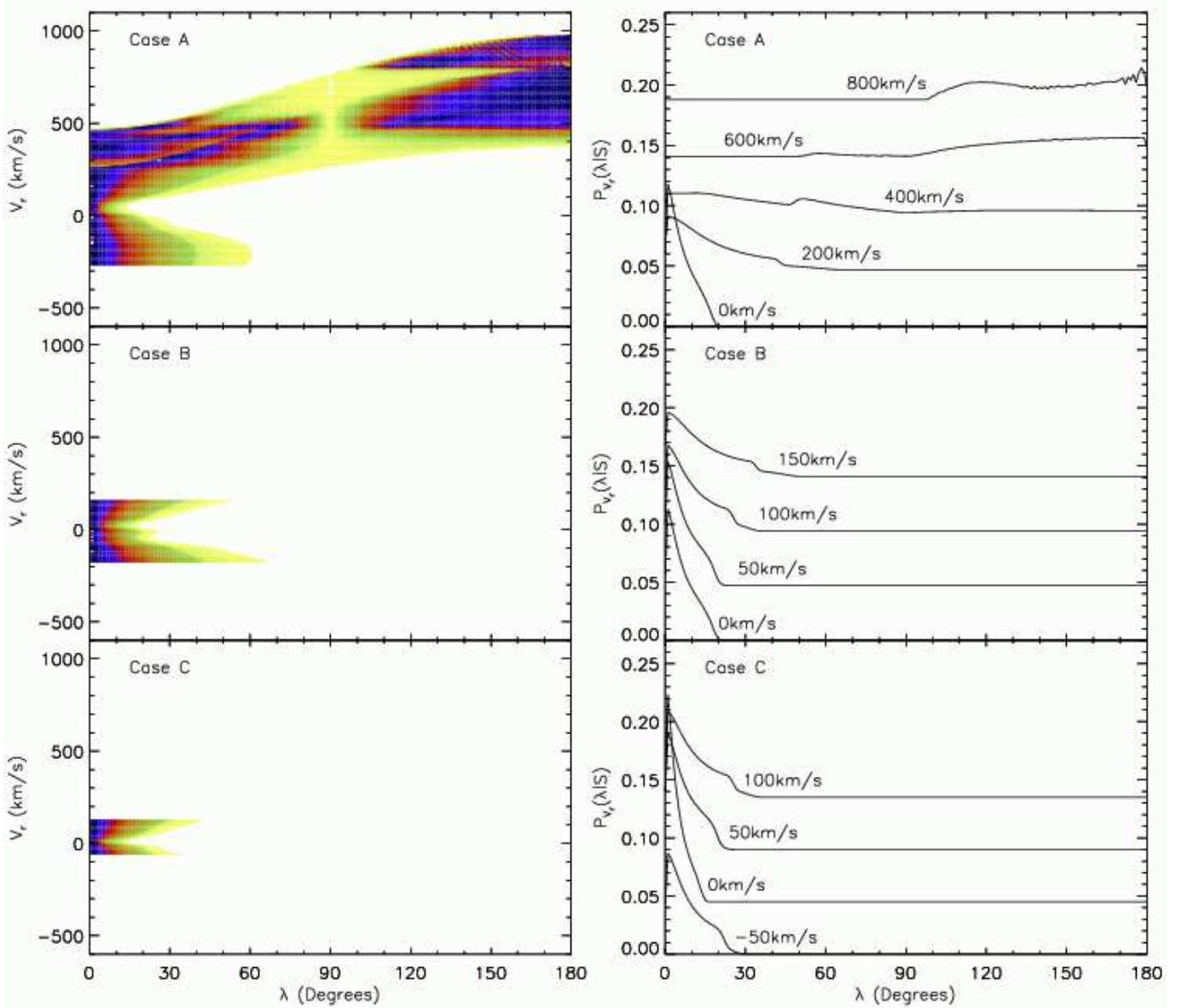


FIG. 19.— Probability distribution functions for the misalignment angle λ between PSR B1534+12's spin axis and the post-SN orbital angular momentum axis, for cases A, B, and C (cf. Fig. 12 for more details).

peaks between $V_k \simeq 50 \text{ km s}^{-1}$ and $V_k \simeq 250 \text{ km s}^{-1}$. For higher radial velocities, relevant only to case A, the peak(s) shift to larger kick velocities up to a maximum of $\simeq 1350 \text{ km s}^{-1}$. The tilt-angle distributions, on the other hand, favor misalignment angles below 30° when $|V_r| \lesssim 200 \text{ km s}^{-1}$ and above 100° when $|V_r| \gtrsim 600 \text{ km s}^{-1}$. For case A disk crossings, tilt angles close to $\lambda \approx 90^\circ$ are furthermore strongly disfavored regardless of the value of the radial velocity. For case B disk crossings, tilt angles with non-vanishing probabilities are always smaller than 40° – 50° .

4. THE RECENT EVOLUTIONARY HISTORY OF PSR B1913+16

Besides the knowledge of the proper motion direction, PSR B1913+16 has the advantage that the misalignment angle between the pulsar's spin axis and the pre-SN orbital angular momentum axis has been determined to be

around $\simeq 20^\circ$, corresponding to prograde rotation, or $\simeq 160^\circ$, corresponding to retrograde rotation (Kramer 1998; Weisberg & Taylor 2002). Wex et al. (2000) used this information to derive constraints on the mass of the second-born NS's direct progenitor, on the pre-SN orbital separation, and on the magnitude and direction of the kick velocity imparted to the second-born NS at birth. In agreement with the then available numerical simulations of rapidly accreting neutron stars, the authors assumed that mass transfer from a helium star companion would cause the NS to collapse into a black hole and therefore excluded Roche-lobe overflowing helium stars as viable progenitors of the second-born NS. However, more recent calculations by Dewi et al. (2002), Ivanova et al. (2003), and Dewi & Pols (2003) show that NS binaries may survive a helium-star mass-transfer phase, provided that the ratio of the helium star's mass to the neutron

star's mass is not too extreme ($M_0/M_A \leq 3.5$). In this section, we therefore revise the constraints derived by Wex et al. (2000) in the light of this new information. The adopted physical parameters are listed in Table 1. The constraints on the tilt angle, for which we consider the values $\lambda = 18^\circ \pm 6^\circ$ and $\lambda = 162^\circ \pm 6^\circ$, are imposed by means of Eq. (14).

We look for possible birth sites of PSR B1913+16 by tracing the system's motion in the Galaxy backwards in time up to a maximum age of 80 Myr⁵, as a function of the unknown radial velocity V_r . In agreement with Wex et al. (2000), we find that the system may have crossed the Galactic plane up to two times. The first Galactic plane crossing (case A) occurs at very young kinematic ages of $\simeq 2\text{--}4$ Myr and gives rise to peculiar velocities in excess of $\simeq 300 \text{ km s}^{-1}$. The corresponding post-SN orbital parameters are $A \approx 2.8 R_\odot$ and $e \approx 0.618$. The second Galactic plane crossing (case B), on the other hand, takes place at least $\simeq 55$ Myr in the past and yields peculiar velocities of $\simeq 230\text{--}440 \text{ km s}^{-1}$. The associated post-SN orbital separations and eccentricities range from $A = 3.1 R_\odot$ and $e = 0.646$ to $A = 3.2 R_\odot$ and $e = 0.658$.

The constraints on the pre-SN parameter space accessible to the progenitor of PSR B1913+16 are shown in Fig. 20 as functions of the unknown radial velocity V_r . As before, the dark gray (red in the electronic edition) regions correspond to the solutions for which no mass transfer takes place at the time of the second SN explosion, while the light gray (blue in the electronic edition) regions indicate the additional solutions found when the possibility of mass transfer is taken into account. The constraints for detached pre-SN binary configurations are in good agreement with the constraints derived by Wex et al. (2000). It is clear however, that when the possibility of mass transfer is taken into account, the available parameter space becomes much less constrained.

For case A disk crossings, the range of radial velocities for which physically acceptable solutions exist is restricted to $|V_r| \lesssim 500\text{--}600 \text{ km s}^{-1}$ when $\lambda = 18^\circ$, and to $100 \text{ km s}^{-1} \lesssim |V_r| \lesssim 1300 \text{ km s}^{-1}$ when $\lambda = 162^\circ$. The mass of the second-born NS's direct progenitor is constrained to the interval between $2.1 M_\odot$ and $8 M_\odot$, and the pre-SN orbital separation to the interval between $1.1 R_\odot$ and $5.3 R_\odot$ for both considered values of the tilt angle λ . The magnitude of the kick velocity varies from $\simeq 190 \text{ km s}^{-1}$ to $\simeq 600 \text{ km s}^{-1}$ when $\lambda = 18^\circ$ and from $\simeq 580 \text{ km s}^{-1}$ to $\simeq 2000 \text{ km s}^{-1}$ when $\lambda = 162^\circ$. When the solutions are restricted to detached pre-SN binary configurations the limits become $300 \text{ km s}^{-1} \lesssim V_k \lesssim 600 \text{ km s}^{-1}$ and $700 \text{ km s}^{-1} \lesssim V_k \lesssim 1250 \text{ km s}^{-1}$ for $\lambda = 18^\circ$ and $\lambda = 162^\circ$, respectively. The direction of the kick velocity is most constrained when $\lambda = 162^\circ$: for $\lambda = 18^\circ$ we have $95^\circ \lesssim \theta \lesssim 175^\circ$ and $5^\circ \lesssim |90^\circ - \xi| \lesssim 85^\circ$, while for $\lambda = 162^\circ$ we find $160^\circ \lesssim \theta \lesssim 175^\circ$ and $5^\circ \lesssim |90^\circ - \xi| \lesssim 15^\circ$. When the parameter space is restricted to detached pre-SN binary configurations, the limits become $145^\circ \lesssim \theta \lesssim 175^\circ$ and $5^\circ \lesssim |90^\circ - \xi| \lesssim 15^\circ$ for $\lambda = 18^\circ$, and $165^\circ \lesssim \theta \lesssim 175^\circ$ and $|90^\circ - \xi| \approx 5^\circ$ for

$\lambda = 162^\circ$.

For case B disk crossings, the mass M_0 of the second-born NS's direct progenitor and the pre-SN orbital separation A_0 are constrained to the ranges of values given by $2.1 M_\odot \lesssim M_0 \lesssim 8 M_\odot$ and $1.1 R_\odot \lesssim A_0 \lesssim 5.3 R_\odot$ when $\lambda = 18^\circ$, and to $2.1 M_\odot \lesssim M_0 \lesssim 5 M_\odot$ and $2.9 R_\odot \lesssim A_0 \lesssim 5.3 R_\odot$ when $\lambda = 162^\circ$. The magnitude of the kick velocity varies between $\simeq 190 \text{ km s}^{-1}$ and $\simeq 530 \text{ km s}^{-1}$ when $\lambda = 18^\circ$, and between $\simeq 550 \text{ km s}^{-1}$ and $\simeq 850 \text{ km s}^{-1}$ when $\lambda = 162^\circ$. When the solutions are restricted to those where no Roche-lobe overflow occurs at the time of the helium star's SN explosion, the minimum kick velocity associated with $\lambda = 18^\circ$ increases slightly to approximately 280 km s^{-1} , while the range of admissible kick velocities associated with $\lambda = 162^\circ$ becomes very tightly constrained to $V_k \approx 640\text{--}680 \text{ km s}^{-1}$. The direction of the kick is again most tightly constrained when $\lambda = 162^\circ$: for $\lambda = 18^\circ$ we have $80^\circ \lesssim \theta \lesssim 175^\circ$ and $|90^\circ - \xi| \gtrsim 5^\circ$, while for $\lambda = 162^\circ$ we find $160^\circ \lesssim \theta \lesssim 175^\circ$ and $5^\circ \lesssim |90^\circ - \xi| \lesssim 10^\circ$. When the parameter space is restricted to detached pre-SN binary configurations, θ and ξ are constrained to $140^\circ \lesssim \theta \lesssim 175^\circ$ and $5^\circ \lesssim |90^\circ - \xi| \lesssim 15^\circ$ for $\lambda = 18^\circ$, and to $\theta \approx 170^\circ\text{--}175^\circ$ and $|90^\circ - \xi| \approx 5^\circ$ for $\lambda = 162^\circ$.

Hence, for both case A and B and for both possible tilt angles λ , the formation of PSR B1913+16 can only be explained if the kicks imparted to the second-born NS are "elevated" out of the orbital plane by at least 5° . In addition, the constraints on θ and ξ imply that a large tilt angle of 162° cannot be obtained if the kicks are perpendicular to the pre-SN orbital plane (i.e. aligned or anti-aligned with the pre-SN orbital angular momentum vector). Instead, for an unambiguous determination of a large tilt angle λ , our results would be more compatible with the findings of Deshpande, Ramachandran, & Radhakrishnan (1999) and Birkel & Toldrà (1997) who argue against a spin-kick correlation.

The inclusion of pre-SN binary configurations for which stable mass transfer occurs from a helium star to the first-born NS furthermore considerably increases the available parameter space for the formation of PSR B1913+16. This is especially true for the prograde case, $\lambda = 18^\circ$, for which the kick direction is no longer required to be close to the pre-SN orbital plane as was found by Wex et al. (2000). The conclusion by Wex et al. (2000) that the retrograde case, $\lambda = 162^\circ$, requires more fine-tuning in the kick direction than the prograde case remains valid even when the possibility of pre-SN Roche-lobe overflow is taken into account.

The probability distribution functions for the magnitude of the kick velocity imparted to the second-born NS in PSR B1913+16 are shown in Fig 21 for both $\lambda = 18^\circ$ and $\lambda = 162^\circ$. The distributions generally show a single peak at kick velocities which increase with increasing absolute values of V_r . For $\lambda = 18^\circ$, the most probable kick velocity ranges from $\simeq 300 \text{ km s}^{-1}$ to $\simeq 600 \text{ km s}^{-1}$, while for $\lambda = 162^\circ$ it ranges from $\simeq 600 \text{ km s}^{-1}$ to almost $\simeq 2000 \text{ km s}^{-1}$.

As a test, we also constructed tilt-probability distributions for PSR B1913+16 by omitting the tilt-angle constraints from the derivation of the admissible parameter space. For case A, the distribution functions peak at $\lambda \lesssim 30^\circ$ when $|V_r| \lesssim 400 \text{ km s}^{-1}$ and at $\lambda \gtrsim 150^\circ$ when $|V_r| \gtrsim 900 \text{ km s}^{-1}$. Intermediate absolute values of the

⁵ As for PSR J0737-3039 and PSR B1534+12, we use the spin-down age $\tau_b = 80$ Myr instead of the characteristic age $\tau_c = 110$ Myr as an upper limit for the age of the system. The maximum amount of orbital evolution that may have taken place since the formation of the DNS is therefore somewhat smaller than in Wex et al. (2000).

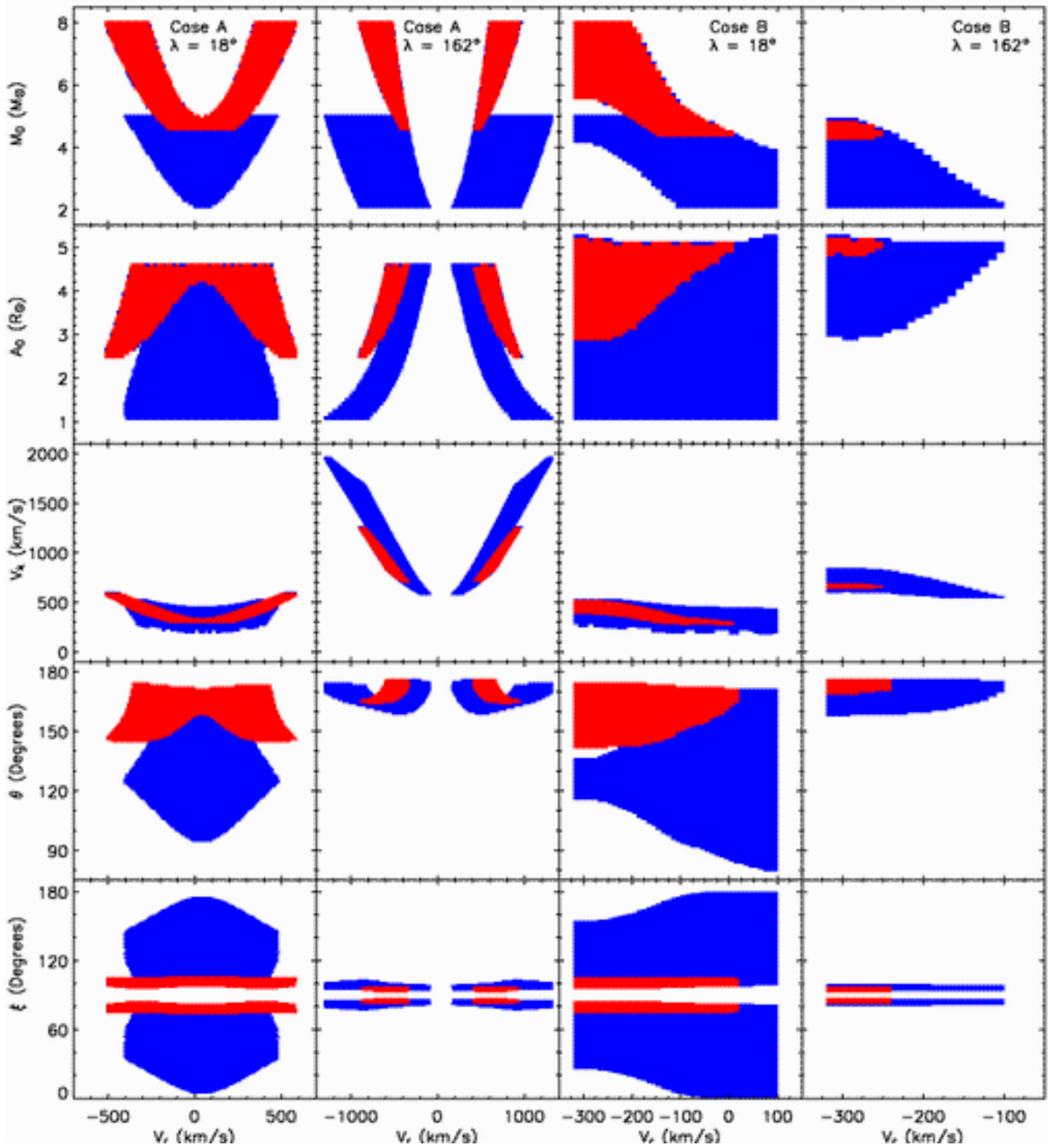


FIG. 20.— Limits on the pre-SN progenitor of PSR B1913+16 and on the kick velocity imparted to the last-born NS. Dark gray (red in the electronic edition) regions correspond to solutions for which the pre-SN binary is detached, while light gray (blue in the electronic edition) regions indicate the additional solutions associated with mass-transferring systems.

radial velocity yield predictions for the tilt angle which are incompatible with the observationally derived values. For case B, the distributions peak at tilt angles $\lambda \lesssim 30^\circ$ and become vanishingly small for $\lambda \gtrsim 30^\circ$ over the entire range of possible V_r -values (see Fig. 20). A large tilt angle of $\lambda = 162^\circ$ can therefore only be explained

if the system has crossed the Galactic plane only once, which would imply that its age is of the order of *only a few Myr*. It is also interesting to note that a tilt angle of 18° would be most favored for radial velocities around -300 km s^{-1} and $+400 \text{ km s}^{-1}$, and a tilt angle of 162° for any radial velocity smaller than -900 km s^{-1} or larger

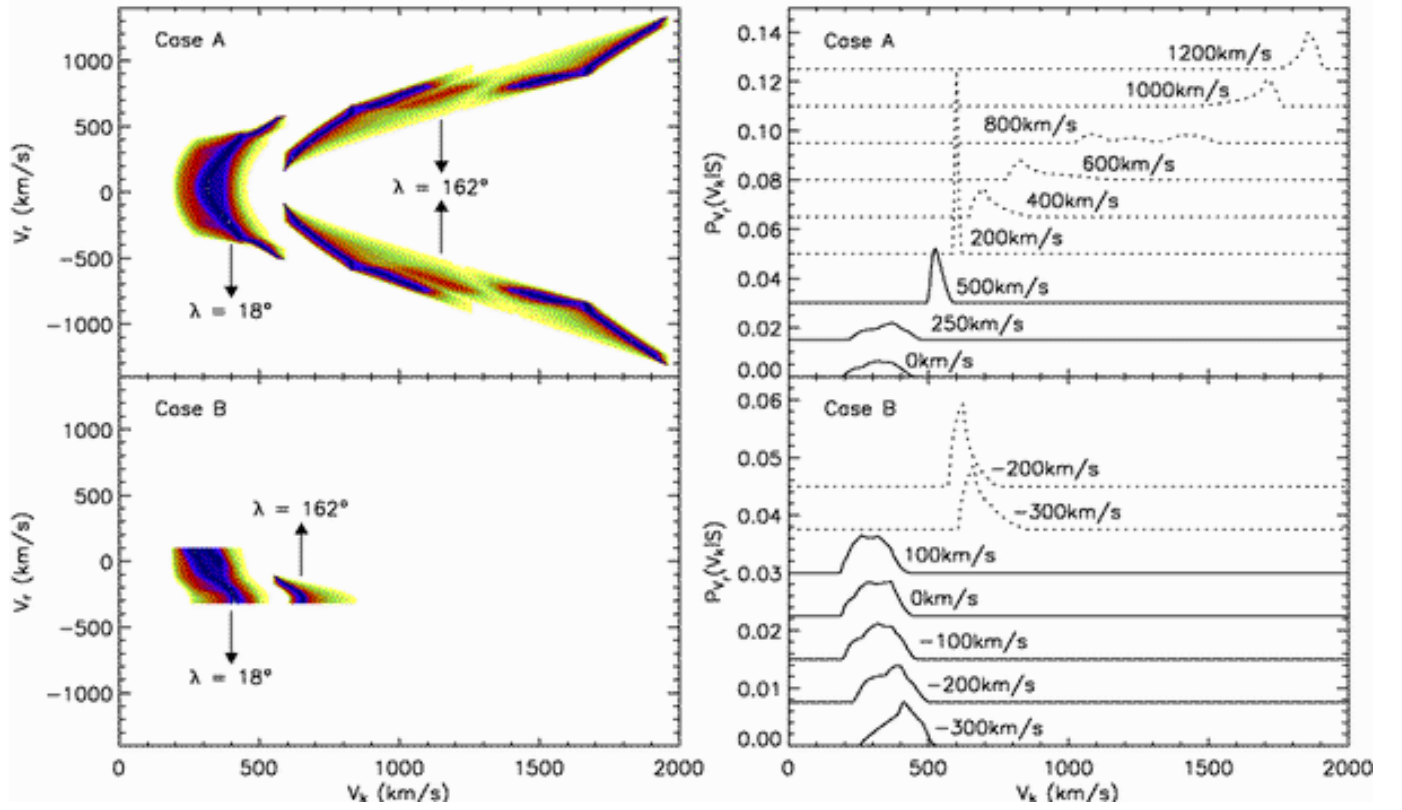


FIG. 21.— Probability distribution functions of the magnitude of the kick velocity imparted to PSR B1913+16’s companion at the time of its formation, for both $\lambda = 18^\circ$ and $\lambda = 162^\circ$ (cf. Fig. 11 for more details). In the right-hand panels, the solid lines correspond to $\lambda = 18^\circ$ and the dashed lines to $\lambda = 162^\circ$.

than $+900 \text{ km s}^{-1}$.

5. CONCLUSIONS AND DISCUSSION

In this paper, we have extended the investigation by Willems & Kalogera (2004) and have derived a more elaborate and tighter set of constraints for the progenitor of PSR J0737-3039 just before the SN explosion that forms the second NS as well as for the magnitude and the direction of the kick imparted to this NS at birth. The additional constraints stem from the kinematic history of the system which is derived by tracing the system’s motion in the Galaxy backwards in time and by assuming that its peculiar velocity results entirely from the second SN explosion. In order to trace the system’s motion backwards in time, we use the scintillation velocity measurements carried out by Ransom et al. (2004), which yield two velocity components in the plane perpendicular to the line-of-sight. Since the orientation of the velocity components is unknown, their orientation Ω in the plane perpendicular to the line-of-sight introduces the first free parameter in the problem. In order to fully describe the system’s space motion, the scintillation velocity components must furthermore be supplemented with the system’s unknown radial velocity V_r , the second free parameter in the problem.

We find that, depending on the values of Ω and V_r , the system may have crossed the Galactic plane up to two times. We identify these crossings as possible birth sites of PSR J0737-3039 and use the times of the crossings as estimates for the system’s age. It follows that there is

a wide range of Ω - and V_r -values for which PSR J0737-3039 may be remarkably young ($\lesssim 20 \text{ Myr}$). If the system has crossed the Galactic plane twice, it is at least 20 Myr old regardless of the values of Ω and V_r . Our kinematical analysis furthermore shows that the post-SN peculiar velocity must have been at least on the order of $\simeq 90 \text{ km s}^{-1}$ and may even have been as high as $\simeq 1200 \text{ km s}^{-1}$ (see Fig. 5). This is in contrast to the work done by Piran & Shaviv (2004) who used the present proximity of the system to the Galactic plane to derive a statistical 95% confidence upper limit of $\simeq 150 \text{ km s}^{-1}$ on the post-SN peculiar velocity.

Next, we used the age estimates and peculiar velocities associated with the Galactic plane crossings to impose additional constraints on the progenitor and formation of PSR J0737-3039 besides those already discussed in Willems & Kalogera (2004). We find that despite the two degrees of freedom, the pre-SN and kick parameters as well as the age become much more constrained for many combinations of Ω and V_r (see Figs. 6–8). An overview of the constraints on the mass M_0 of pulsar B’s helium star progenitor, the pre-SN orbital separation A_0 , and the magnitude V_k of the kick velocity imparted to pulsar B at birth as a function of V_r for all possible values of Ω is given in Fig. 22. The absolute limits covering the whole range of admissible Ω - and V_r -values are summarized in Table 2.

We also examined constraints on the kick direction in terms of the angle θ between the kick direction and the pre-SN orbital velocity of pulsar B’s helium star pro-

TABLE 2
SUMMARY OF THE CONSTRAINTS DERIVED FOR PSR J0737-3039, PSR B1534+12, AND PSR B1913+16. FOR PSR B1534+12, AND PSR B1913+16 NUMBERS BETWEEN PARENTHESES CORRESPOND TO THE CONSTRAINTS ASSOCIATED WITH DETACHED PRE-SN PROGENITORS.

Parameter	PSR J0737-3039	PSR B1534+12	PSR B1913+16	
			$\lambda^f = 18^\circ \pm 6^\circ$	$\lambda^f = 162^\circ \pm 6^\circ$
M_0 (M_\odot) ^a	2.1–4.7	2.1–8.0 (4.7–8.0)	2.1–8.0 (4.5–8.0)	2.1–8.0 (4.5–8.0)
A_0 (R_\odot) ^b	1.2–1.7	2.4–4.3 (2.5–4.3)	1.1–5.3 (2.5–5.3)	1.1–5.3 (2.5–5.3)
V_k (km s^{-1}) ^c	60–1660	15–1350 (230–1350)	190–600 (300–600)	580–2000 (700–1250)
θ (degrees) ^d	115–180	95–180 (140–180)	95–175 (145–175)	160–175 (165–175)
ξ (degrees) ^e	25–155	5–175 (55–125)	5–85 or 95–175 (75–85 or 95–105)	75–85 or 95–105 (≈ 85 or ≈ 95)

^aPre-SN mass of the last-born NS’s helium star progenitor.

^bPre-SN orbital separation.

^cKick-velocity magnitude.

^dAngle between the kick direction and the pre-SN orbital velocity of the last-born NS’s helium star progenitor.

^eAngle between the kick direction and the pre-SN orbital angular momentum axis.

^fMisalignment angle between PSR B1913+16’s spin axis and the post-SN orbital angular momentum axis.

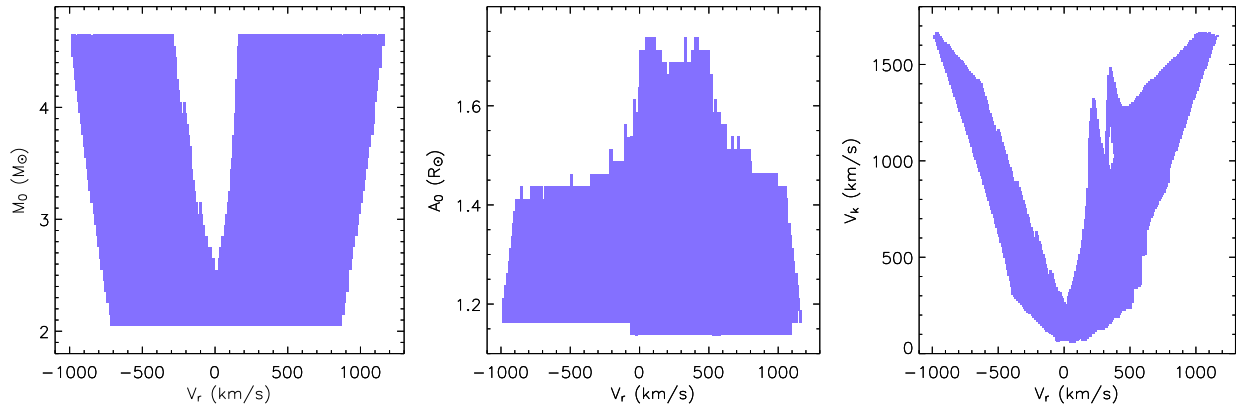


FIG. 22.— Overview of the constraints on the mass M_0 of PSR J0737-3039B’s helium star progenitor, the pre-SN orbital separation A_0 , and the magnitude V_k of the kick velocity imparted to pulsar B at birth, as a function of V_r for all possible values of Ω .

genitor, as well as the angle ξ between the kick direction and the pre-SN orbital angular momentum vector (which could be associated with pulsar B’s spin axis). We find that θ is always larger than $\simeq 115^\circ$, while ξ ranges from $\simeq 25^\circ$ to $\simeq 155^\circ$. The kick imparted to pulsar B at birth must therefore have been directed opposite to the orbital motion and cannot have been too closely aligned with the pre-SN orbital angular momentum axis.

For each combination of Ω and V_r yielding viable progenitors for PSR J0737-3039, we derived probability distributions for the magnitude of the kick velocity under the assumption that all kick directions are equally probable (Fig. 11). The distribution functions exhibit a single peak at kick velocities which increase from $\simeq 100 \text{ km s}^{-1}$ to $\simeq 1600\text{--}1700 \text{ km s}^{-1}$ with increasing absolute values of the radial velocity. This is in contrast to Willems & Kalogera (2004) who found a single most probable kick velocity of $\simeq 150 \text{ km s}^{-1}$. The dependence of the position of the peak on the radial velocity found here stems from the relation between the kick magnitude and the post-SN peculiar velocity which tends to select those kick velocities which are able to explain the system’s motion in the Galaxy (high space velocities cannot be explained by low kick velocities and vice versa). However, for a given radial velocity, the range of kick velocities

with non-vanishingly small probabilities found here is always much more constrained than in Willems & Kalogera (2004).

Similarly, we derived distribution functions for the misalignment angle λ between pulsar A’s spin axis and the post-SN orbital angular momentum axis (Fig. 12). Tilt angles lower than $30^\circ\text{--}50^\circ$ are clearly favored in the cases where (i) the system has crossed the Galactic plane twice in the past and (ii) the system crossed the Galactic plane once and has a current radial velocity of less than $\simeq 500 \text{ km s}^{-1}$ in absolute value. Higher tilt angles must be associated with one disk crossing and much higher present-day radial velocities of $\simeq 500\text{--}1200 \text{ km s}^{-1}$ in absolute value. Tilt angles close to 90° are furthermore strongly disfavored for any radial velocity V_r . Our probability distributions are thus compatible with the tilt-angle predictions of $16^\circ \pm 10^\circ$ and $164^\circ \pm 10^\circ$ made by Jenet & Ransom (2004) and with the spin- magnetic dipole misalignment angle derived by Demorest et al. (2004) which rules out Jenet & Ransom’s alternative solutions of $82^\circ \pm 16^\circ$ or $98^\circ \pm 16^\circ$.

In view of recent claims of alignment of NS kicks with NS spin axes (e.g. Romani 2004), we also considered kick-velocity and tilt-angle distributions for polar kicks where the kick direction is confined within two oppo-

sitely directed cones with an opening angle of 30° and with axes parallel to the pre-SN orbital angular momentum axis (i.e. $\xi \leq 30^\circ$). The confinement of the kick directions strongly reduces the range of radial velocities for which viable progenitors for PSR J0737-3039 may be found. Correspondingly, the range of most probable kick velocities shrinks to $\simeq 200\text{--}550\text{ km s}^{-1}$, and the range of most probable tilt angles to $15^\circ\text{--}45^\circ$ (see Figs. 14 and 15).

Progenitor constraints and isotropic kick-velocity and spin-tilt distributions were also derived for PSR B1534+12 and PSR B1913+16. Both systems have a measured proper motion with a known direction in the plane of the sky, so that the derived constraints and probability distributions only depend on the unknown radial velocity V_r . For PSR B1913+16, the knowledge of the tilt angle λ (Kramer 1998; Weisberg & Taylor 2002) furthermore puts additional constraints on the possible progenitor systems, which are not yet available for PSR J0737-3039 and PSR B1534+12.

The absolute limits on the pre-SN binary and kick parameters of the two systems are summarized in Table 2 (the dependency of the constraints on V_r is shown Figs. 17 and 20). Contrary to PSR J0737-3039, the progenitors of these two systems were not necessarily undergoing a mass-transfer phase at the time the second NS was born. The helium star masses M_0 , pre-SN orbital separations A_0 , and kick velocities V_k associated with detached progenitors are, however, always much more constrained than those associated with the full set of detached and semi-detached progenitors. In particular, the possibility of pre-SN Roche-lobe overflow considerably relaxes the constraints on the progenitor of PSR B1913+16 derived by Wex et al. (2000).

The constraints on the direction of the kick imparted to the second-born NS in PSR B1534+12 and PSR B1913+16 yield very similar conclusions as for PSR J0737-3039: the kicks are generally directed oppositely to the orbital motion and cannot have been too closely aligned with the pre-SN orbital angular momentum axis.

The kick-velocity and spin-tilt distributions for PSR B1534+12 and PSR B1913+16 (Figs. 18, 19 and 21) also show qualitatively the same behavior as for PSR J0737-3039. The most probable kick velocity depends on the unknown radial velocity and, depending on the value of V_r , can be anywhere between the derived lower and upper limits for the kick imparted to the second-born NS. Tilt angles smaller than $30^\circ\text{--}50^\circ$ are again favored when (i) the system crossed the Galactic plane more than once and (ii) the system crossed the Galactic plane once and has a current radial velocity smaller than $\simeq 250\text{ km s}^{-1}$ in absolute value for PSR B1534+12 and smaller than $\simeq 500\text{ km s}^{-1}$ in absolute value for PSR B1913+16.

For conclusion, we point out that the set of observational measurements and constraints available for double neutron stars systems are sufficient to greatly limit the properties of the progenitors. As a follow-up investigation it will be therefore interesting to compare these strongly constrained progenitor properties to synthesis studies of binary populations and double neutron star formation.

We are grateful to Scott Ransom for sharing the scintillation velocity measurements for PSR J0737-3039 prior to publication; to Ingrid Stairs for pointing out the correct measurements of the proper motion of PSR B1534+12 before the publication of the paper; to Steve Thorsett for helping us identify a sign error in the Galactic motion calculations for PSR B1534+12; and to Laura Blecha for sharing the code used to trace the motion of the DNS binaries in the Galactic potential. We also thank the referee, Philipp Podsiadlowski, for his useful suggestions and remarks which helped to improve the paper. The organizers of the Aspen Winter Conference on Binary Radio Pulsars are acknowledged for putting together a stimulating conference during which this research was initiated. This work is partially supported by a NSF Gravitational Physics grant, a David and Lucile Packard Foundation Fellowship in Science and Engineering grant, and NASA ATP grant NAG5-13236 to VK.

REFERENCES

- Arons, J., Backer, D.C., Spitkovski, A., & Kaspi, V.M. 2004, in *Binary Radio Pulsars*, proceedings of an Aspen Winter Conference, eds. F. Rasio and I. Stairs, in press
- Arzoumanian, Z., Cordes, J.M., & Wasserman, I. 1999, *ApJ*, 520, 696
- Belczynski, K., Kalogera, V., & Bulik, T. 2002, *ApJ*, 572, 407
- Bevington, Ph.R. & Robinson, D.K. 2002, *Data Reduction and Error Analysis for the Physical Sciences*, McGraw-Hill Science/Engineering/Math, 3rd edition
- Bienaymé, O. 1999, *A&A*, 341, 86
- Binney, J. & Dehnen, W. 1997, *MNRAS*, 287, L5
- Birkel, M. & Toldrà, R. 1997, *A&A*, 326, 995
- Brandt, N. & Podsiadlowski, Ph. 1995, *MNRAS*, 274, 461
- Burgay, M., et al. 2003, *Nature*, 426, 531
- Damour, T. & Taylor, J.H. 1991, *ApJ*, 366, 501
- Demorest, P., Ramachandran, R., Backer, D.C., Ransom, S.M., Kaspi, V., Arons, J., & Spitkovsky, A. 2004, *ApJL*, submitted (astro-ph/0402025)
- Deshpande, A.A., Ramachandran, R., & Radhakrishnan, V. 1999, *A&A*, 351, 195
- Dewi, J.D.M. & Pols, O.R. 2003, *MNRAS*, 344, 629
- Dewi, J.D.M. & van den Heuvel, E.P.J. 2004, *MNRAS*, 349, 169
- Dewi, J.D.M., Pols, O.R., Savonije, G.J., & van den Heuvel, E.P.J. 2002, *MNRAS*, 331, 1027
- Flannery, B.P. & van den Heuvel, E.P.J. 1975, *A&A*, 39, 61
- Fryer, C. & Kalogera, V. 1997, *ApJ*, 489, 244
- Granot, J. & Mészáros, P. 2004, *ApJL*, 609, L17
- Hills, J.J. 1983, *ApJ*, 267, 322
- Hulse, R.A. & Taylor, J.H. 1975, *ApJL*, 195, L51
- Ivanova, N., Belczynski, K., Kalogera, V., Rasio, F.A., & Taam, R.E. 2003, *ApJ*, 592, 475
- Jenet, F.A. & Ransom, S.M. 2004, *Nature*, 428, 919
- Junker, W. & Schäfer, G. 1992, *MNRAS*, 254, 146
- Kalogera, V. 1996, *ApJ*, 471, 352
- Kalogera, V. 2000, *ApJ*, 541, 319
- Kalogera, V. & Lorimer, D.R. 2000, *ApJ*, 530, 890
- Kalogera, V., et al. 2004, *ApJL*, 601, L179
- Kim, C., Kalogera, V., Lorimer, D.R., Ihm, M., & Belczynski, K. 2004, in *Binary Radio Pulsars*, proceedings of an Aspen Winter Conference, eds. F. Rasio and I. Stairs, in press (astro-ph/0405564)
- Konacki, M., Wolszczan, A., & Stairs, I.H. 2003, *ApJ*, 589, 495
- Kramer, M. 1998, *ApJ*, 509, 856
- Kramer, M., et al. 2004, in *Binary Radio Pulsars*, proceedings of an Aspen Winter Conference, eds. F. Rasio and I. Stairs, in press (astro-ph/0405179)
- Kuijken, K. & Gilmore, G. 1989, *MNRAS*, 239, 571
- Kuijken, K. & Rich, R.M. 2002, *AJ*, 124, 2054
- Lai, D., Chernoff, D.F., & Cordes, J.M. 2001, *ApJ*, 549, 1111
- Lorimer, D.R., et al. 2004, in *Binary Radio Pulsars*, proceedings of an Aspen Winter Conference, eds. F. Rasio and I. Stairs, in press (astro-ph/0404274)

- Lyne, A.G., et al. 2004, *Science*, 303, 1153
- Lyutikov, M. 2004, *MNRAS*, 353, 1095
- McLaughlin, M.A., et al. 2004, *ApJL*, 605, L41
- Pfahl, E., Rappaport, S., Podsiadlowski, Ph., & Spruit, H. 2002, *ApJ*, 574, 364
- Piran, T. & Shaviv, N.J. 2004, *ArXiv Astrophysics e-prints* (astro-ph/0401553)
- Ransom, S.M., et al. 2004, *ApJL*, 609, L71
- Romani, R.W. 2004, in *Binary Radio Pulsars*, proceedings of an Aspen Winter Conference, eds. F. Rasio and I. Stairs, in press (astro-ph/0404100)
- Stairs, I.H., Thorsett, S.E., Taylor, J.H., & Wolszczan, A. 2002, *ApJ*, 581, 501
- Tauris, T.M. & van den Heuvel, E.P.J. 2004, in *Compact Stellar X-ray Sources*, Eds. W.H.G. Lewin & M. van der Klis, (Cambridge: Cambridge University Press), astro-ph/0303456
- Taylor, J.H., Fowler, L.A., & McCulloch, P.M. 1979, *Nature*, 277, 437
- Taylor, J.H., Hulse, R.A., Fowler, L.A., Gullahorn, G.E., & Rankin, J.M. 1976, *ApJL*, 206, L53
- Taylor, J.H. & Weisberg, J.M. 1982, *ApJ*, 253, 908
- Taylor, J.H. & Weisberg, J.M. 1989, *ApJ*, 345, 434
- Wex, N., Kalogera, V., & Kramer, M. 2000, *ApJ*, 528, 401
- Weisberg, J.M. & Taylor, J.H. 2002, *ApJ*, 576, 942
- Willems, B. & Kalogera, V. 2004, *ApJL*, 603, L101
- Wolszczan, A. 1991, *Nature*, 350, 688